Applied Catalysis B: Environmental 227 (2018) 386–408

Contents lists available at ScienceDirect

Applied Catalysis B: Environmental

journal homepage: www.elsevier.com/locate/apcatb

Review

Review on selective hydrogenation of nitroarene by catalytic, photocatalytic and electrocatalytic reactions

Jiajia Song[1], Zhen-Feng Huang[1], Lun Pan, Ke Li, Xiangwen Zhang, Li Wang, Ji-Jun Zou*

Key Laboratory for Green Chemical Technology of the Ministry of Education, School of Chemical Engineering and Technology, Tianjin University, Collaborative Innovative Center of Chemical Science and Engineering (Tianjin), Tianjin 300072, China

ARTICLE INFO

Keyword:
Nitroarene hydrogenation
Photocatalysis
Electrocatalysis
Catalyst
Reaction mechanism

ABSTRACT

Selective catalytic hydrogenation of nitroarenes is of great importance for dyestuff and pharmaceutical industry. A critical step toward the rational design of targeted catalysts is to determine their electronic structures and related reaction mechanism. In this review, we summarize the breakthroughs on the development of multiple catalytic technologies in the past decade, including direct hydrogenation using high-pressure hydrogen; transfer hydrogenation using reductive compounds; photocatalytic hydrogenation using hole scavenger; electrocatalytic hydrogenation accompanied with water oxidation. We focus on how to understand the two key element steps including hydrogen dissociation and the activation of nitro group in the process of hydrogenation, and design and fabricate nanostructured catalysts with desired activity and selectivity. For direct catalytic hydrogenation, representative catalysts include metal, metal oxide/sulfide/carbides/nitrides/boride, and functional carbon material, and the crucial factors to tune their activity and selectivity are discussed such as metal-support interaction, size effect, alloy effect, defect engineering, and so on. Catalytic transfer hydrogenation, photocatalytic and electrocatalytic hydrogenation, in which these catalysts abstracts hydrogen species from the hydrogen donor and stabilizes it on the catalyst surface, restricting active H* recombination, and then the active hydrogen species can be promptly transferred to nitroarenes for the hydrogenation. It is worth mentioning that the light harvesting and charge separation of photocatalyst and the conductivity of electrocatalyst should also be considered together for the overall performance. All these experiences lay the foundation for large scale production of anilines and guide the rational design of catalysts for other organic transformation reactions.

1. Introduction

The transformation of nitroarenes to anilines is of great importance because anilines are among the most important intermediates necessary for dyestuffs and pharmaceuticals in chemical industry [1–5]. Currently, the commercial production of functionalized anilines mainly depends on non-catalytic reduction of nitroarenes using stoichiometric reducing agents such as sodium hydrosulfite, iron, tin or zinc in ammonium hydroxide [6]. Such processes, however, have serious environmental issues and suffer from poor selectivity. Therefore, the development of more efficient, selective and environmentally friendly process to produce anilines is important for both fundamental studies and industrial applications.

Catalytic hydrogenation using high-pressure hydrogen with supported precious metal such as Pt as catalyst is a preferred choice [1]. Nevertheless, the selective hydrogenation of nitro groups but not functional groups (e.g., −OH, −Cl, −C═O, −C═C) remains a great challenge. Corma et al. reported a breakthrough with regard to functional-group tolerance using Au/TiO_2 as catalyst, exhibiting selectivity of over 95% for hydrogenation of nitro group in 3-nitrostyrene, 4-nitrobenzaldehyde, 4-nitrobenzonitrile, and 4-nitrobenzamide [2–5]. They attributed the high selectivity to the metal/support interface of catalyst that regulates the adsorption to preferentially activate $-NO_2$ group. Still the high-cost and limited availability for Au also stimulate numerous efforts in seeking earth-abundant, highly active and stable catalyst with excellent selectivity. In the past decade, many significant and encouraging breakthroughs on non-noble metal catalysts have been made for highly-efficient selective hydrogenation of nitroarenes to anilines. For example, Beller et al. reported catalysts based on abundantly available transition metals, such as Fe, Co and Ni, can mediate selective hydrogenation of nitroarenes efficiently [7–9]. Also, Zhang et al. found atomically dispersed single-atom Co in form of Co−N−C is very active and selective for this reaction. DFT calculations have conducted to explain and predict the reactivity and selectivity of the catalysts, mainly

* Corresponding author.
E-mail address: jj_zou@tju.edu.cn (J.-J. Zou).
[1] J. Song and Z.-F. Huang contributed equally to this work.

https://doi.org/10.1016/j.apcatb.2018.01.052
Received 14 August 2017; Received in revised form 15 December 2017; Accepted 22 January 2018

by estimating the adsorption and dissociation energy of reactant on catalyst surface [10–15]. Besides, some analytical and characterization techniques including Fourier transform infrared spectroscopy (FTIR), Raman spectroscopy, X-ray absorption/diffraction, Mössbauer spectroscopy and so on, allow us to monitor the reaction pathway in situ and confirm the actual active phase/intermediates during the catalytic process [16–19].

Catalytic transfer hydrogenation using hydrogen donors like hydrazine, formic acid, or $NaBH_4$ are also very attractive, because it can be performed in a convenient manner without the requirement of high-pressure equipment and avoid sluggish H_2 activation dynamics. Similarly, photocatalytic and electrocatalytic hydrogenation of nitroarenes under room temperature and atmosphere have recently attracted increasing attentions, which can be driven by solar energy, or solar-, wind- and other renewable resources-derived electricity. In these processes, catalysts are also very necessary to adsorb and activate the nitro groups for proton-coupled electron transfer.

This review describes recent progress on the development of multiple catalytic technologies and design and synthesis of corresponding nanostructured catalytic materials towards selective catalytic hydrogenation of nitroarene. The fundamentals of direct catalytic hydrogenation of nitroarene to aniline including reaction mechanism are first introduced. Then we summarize various types of nanostructured catalysts for catalytic and selective hydrogenation of nitroarenes including metal, metal oxide, sulfide/carbides, nitrides and boride, and functional carbon material. The crucial factors determining the activity and selectivity are discussed, including (1) metal-support interaction, size effect, single-atom catalyst, alloy effect, shape-selective catalysis, strain effect, and interfacial adsorbent-metal interaction of metal; (2) defect engineering and metal oxide/N-doped carbon interaction of metal oxide; (3) interfacial electronic effect of carbon material. All these strategies can tune and optimize the production of reactive hydrogen species and preferential adsorption of nitro group of nitroarenes. In addition, catalytic transfer hydrogenation using reductive compounds such as hydrazine, $NaBH_4$, alcohols and formic acid, photocatalytic hydrogenation using hole scavenger and electrocatalytic hydrogenation accompanied with water oxidation are also reviewed from the aspects of reaction mechanism, design and performance of catalysts.

2. Fundamentals of catalytic hydrogenation of nitroarene

2.1. Reaction mechanism

More than 100 years ago, Haber et al. proposed a reaction network (Fig. 1a) for the hydrogenation of nitrobenzene and substituted nitrobenzene [20], in which nitrosobenzene, phenylhydroxylamine, azobenzene, azoxybenzene, and hydrazobenzene are potential intermediates. They assumed there are equilibria between these species in solution and reversibly adsorbed on the surface of solid catalysts (both the active phase and the support). This mechanistic scheme is an excellent basis to describe how the catalytic hydrogenation proceeds. Usually, only the starting nitroarene, nitroso, hydroxylamine, and aniline products are detected in solution, which is recently confirmed by several kinetic studies by applying online Raman and IR spectroscopic techniques [20]. The nitroso intermediate typically presents in very trace concentration, and hydroxylamine concentration varies considerably depending on such factors as substrate structure, reaction temperature, hydrogen pressure, solvents, catalysts, and pH value. The reaction profile indicates a fast reduction of nitro group to nitroso intermediate that are adsorbed very strongly on metal surface and hydrogenated to hydroxylamine very quickly, and the hydrogenation of hydroxylamine to aniline is the rate-determining step. Condensation to azo and azoxy products does not occur usually, except when a strong base is present, via the intermolecular dehydration between nitrosoarenes and hydroxylamine (Fig. 1a).

In addition to the Haber mechanism, Jackson et al. found that the reaction profiles are different when nitrosobenzene is used as a starting substrate, indicating the nitroso species is not an obligatory intermediate and there might be a direct pathway from nitro group to hydroxylamine [2,21–23]. However, the evidence is rather circumstantial, and no proposal has been made as to how the addition of four H atoms to the nitro group and the loss of one H_2O could proceed in one step. They considered Ph-N(OH) as a common intermediate (Fig. 1b) in nitrobenzene hydrogenation, and then it directly reacts with adsorbed H to produce Ph-NH (accompanied by dehydration) and final $PhNH_2$. However, the Ph-N(OH) intermediate reacts with itself to eliminate water and mainly produce azoxybenzene in nitrosobenzene hydrogenation. As a result, nitrosobenzene as starting substrate has a slower rate of aniline formation.

2.2. Advantages and challenges

Noncatalytic reduction of nitroarenes with stoichiometric reducing agents, such as sulfides, Fe, and Zn, is widely used to produce functionalized anilines in industry [20]. However, these processes generate large amount of waste acids and residues, leading to serious environmental problems. In contrast, catalytic hydrogenation with the supported catalysts is environmentally benign and highly efficient [5,9,24]. Due to the enormous potential rewards, extensive studies have been done for nitroarenes hydrogenation. However, up till now, few catalysts have met the requirements for practical use. Several scientific challenges still remain, such as:

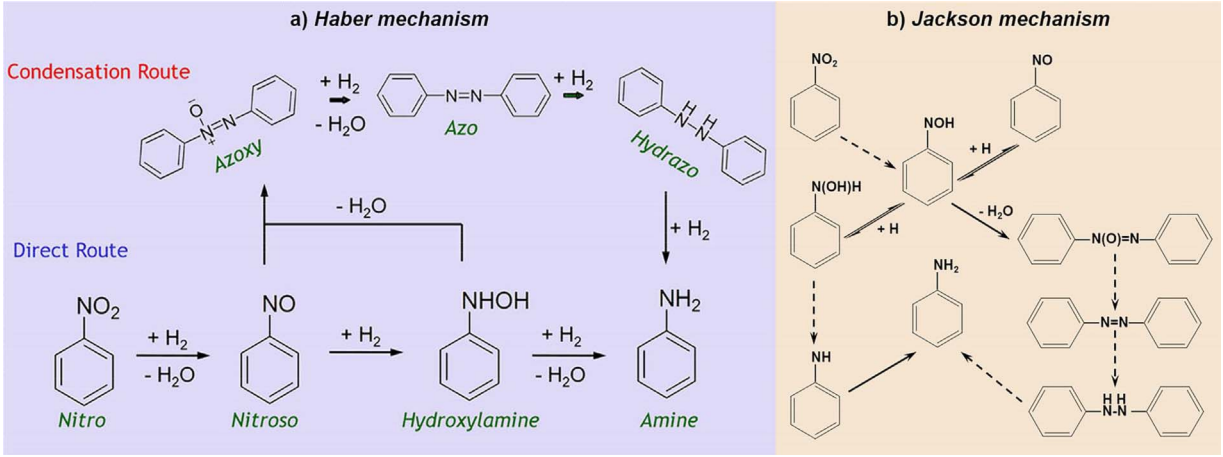

Fig. 1. (a) Haber mechanism for hydrogenation of nitrobenzene. (a reproduced from Ref. [20] with permission. Copyright 2015, American Chemical Society) (b) Jackson mechanism for hydrogenation of nitrobenzene. (b reproduced from Ref. [21] with permission. Copyright 2005, Royal Society of Chemistry).

(1) It is difficult to selectively hydrogenate nitro groups when other groups are present (the latter must be retained to preserve products with high synthetic value). Also, it is difficult to control the degree of hydrogenation of nitro reduction to selectively afford fully hydrogenated amine or, otherwise, a particular intermediate such as hydroxylaniline or azobenzene compounds [25].
(2) It is challenging to obtain both high activity and selectivity since increasing the activity often causes decrease in selectivity.
(3) The reaction mechanism and corresponding active sites for the adsorption of reactant, hydrogen dissociation and subsequent step-by-step hydrogenation are still under debate. More in-situ characterizations and theoretical computation need to be performed.

2.3. Key points behind classical Au/TiO_2 catalysis

2.3.1. Rate-limiting step and active site for hydrogen dissociation

In order to develop a promising, versatile catalyst for the selective hydrogenation of nitroarene, the understanding of rate-limiting step is of great importance. To do that, a thorough kinetic investigation was performed with the classical Au/TiO_2 catalyst to identify the rate-determining step. The reaction rate is observed to decrease with increasing nitrobenzene (NB) concentration in the range 0.2–1.2 mmol/L at 393 K and 8 bar of H_2 in toluene, whereas the dependence is direct and linear with the hydrogen pressure when the nitrobenzene concentration is held at ~0.42 mmol/L [26]. Thus, the adsorption/dissociation of H_2 is the controlling step of the reaction. Assuming Langmuir-Hinshelwood and Hougen-Watson hypotheses ($r = (k_{H2}{\cdot}P_{H2})(1 + K_{NB}{\cdot}C_{NB})^{-2}$, where k_{H2} is kinetic constant of H_2 dissociation, K_{NB} is adsorption constant of nitrobenzene in the equilibrium, P_{H2} is H_2 pressure and C_{NB} is NB concentration.), a clear linear correlation between the conversion of 3-nitrostyrene and the H_2-D_2 exchange for a series of Au/TiO_2 catalysts with different levels of activity, further confirms that the overall reaction is controlled by H_2 dissociation on Au.

Coma et al. further identified the active sites for H_2 adsorption and activation in Au/TiO_2 and the role of reductive support using DFT calculations [27]. They found that the active sites for H_2 dissociation are corner or edge atoms in low coordination state not directly bonded to O of TiO_2 and not belonging to the first atomic layer in contact with the support (Fig. 2a, b) [27]. From the view of catalyst design, the Au particles should have two layer (2L) structure with one bottom layer of Au atoms in contact with the support and therefore inactive, and one top layer separated from the support with low coordinated gold atoms on which H_2 is adsorbed and activated. The role of oxygen defects in TiO_2 is to stabilize these 2L particles.

2.3.2. Selectivity

In addition to H_2 dissociation, the adsorption and activation of $-NO_2$ group are also critical to control the reaction selectivity. Au/TiO_2 is highly selective, whereas Au nanoparticles on supports such as SiO_2 and carbon are unselective for the hydrogenation of nitrostyrene. To uncover the adsorption mode of $-NO_2$ group on catalyst surface, three typical methods can be used, taking 3-nitrostyrene adsorbed on Au/TiO_2 as example [3]. Firstly, DFT computation predicts that the adsorption of $-NO_2$ group prevails over the adsorption of C=C bond (Fig. 2c), and the reaction is simulated to occur at the interface between Au and TiO_2 support. Secondly, IR spectra demonstrates the interaction of nitrobenzene with Au surface is very strong and hinders the adsorption of other groups (such as C=C bonds in styrene) when TiO_2 is the support, but not when SiO_2 is the support. Thirdly, kinetic experiments show a higher intrinsic activity for hydrogenating nitro with respect to olefin group, from the phenomenon that the rate of nitrobenzene hydrogenation by Au/TiO_2 is greater than that of styrene. Similar result is also observed on Pt/TiO_2 for the hydrogenation of 4-chloronitrobenzene (Fig. 2d) [4].

Since nitro group is typically adsorbed more strongly on metal surface than most other functional groups, the surface will be covered by adsorbed nitro groups and the access for other functions is thereby inhibited. This explains why, in many cases, the selectivity decreases as the reaction proceeds gradually due to the decreased coverage of catalyst surface by decreased concentration of reactant in solution [22]. Also, it indicates that controlling the size of metal particles is important to tune the adsorption mode of nitro group. Even though there are no experimental results available, it is generally assumed that the nitro group should be adsorbed parallel to the metal surface in order to be hydrogenated. On large metal particles (and flat surfaces) this means that parallel adsorption will inevitably lead to interaction with other substituted groups. The case may be different if very small metal particles are present or if the metal surface is modified, for example, by a strong metal-support interaction.

2.4. Analysis on metal oxide as potential hydrogenation catalyst

As aforementioned, the effect of reductive support such as TiO_2 and

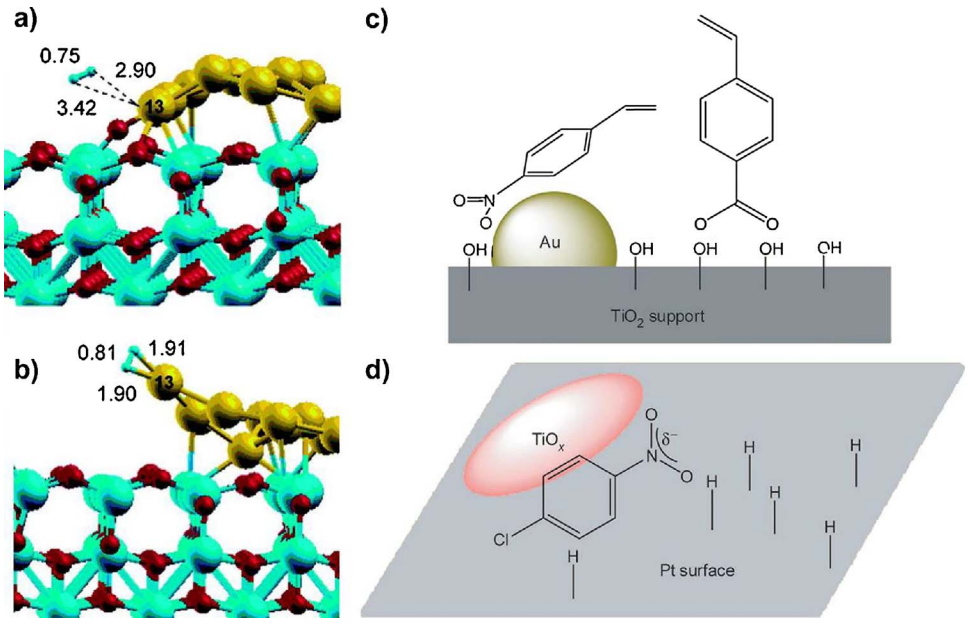

Fig. 2. (a, b) Optimized geometry of H_2 on Au particles supported on 1L-stoichiometric TiO_2 and 1L-reductive TiO_2. (a, b reproduced from Ref. [27] with permission. Copyright 2009, American Chemical Society) (c) Schematic adsorption of 3-nitrostyrene on Au/TiO_2 catalyst. (c reproduced from Ref. [3] with permission. Copyright 2007, American Chemical Society) (d) Schematic adsorption of 4-chloronitrobenzene on Pt/TiO_2 catalyst. (d reproduced from Ref. [4] with permission. Copyright 2007, American Chemical Society).

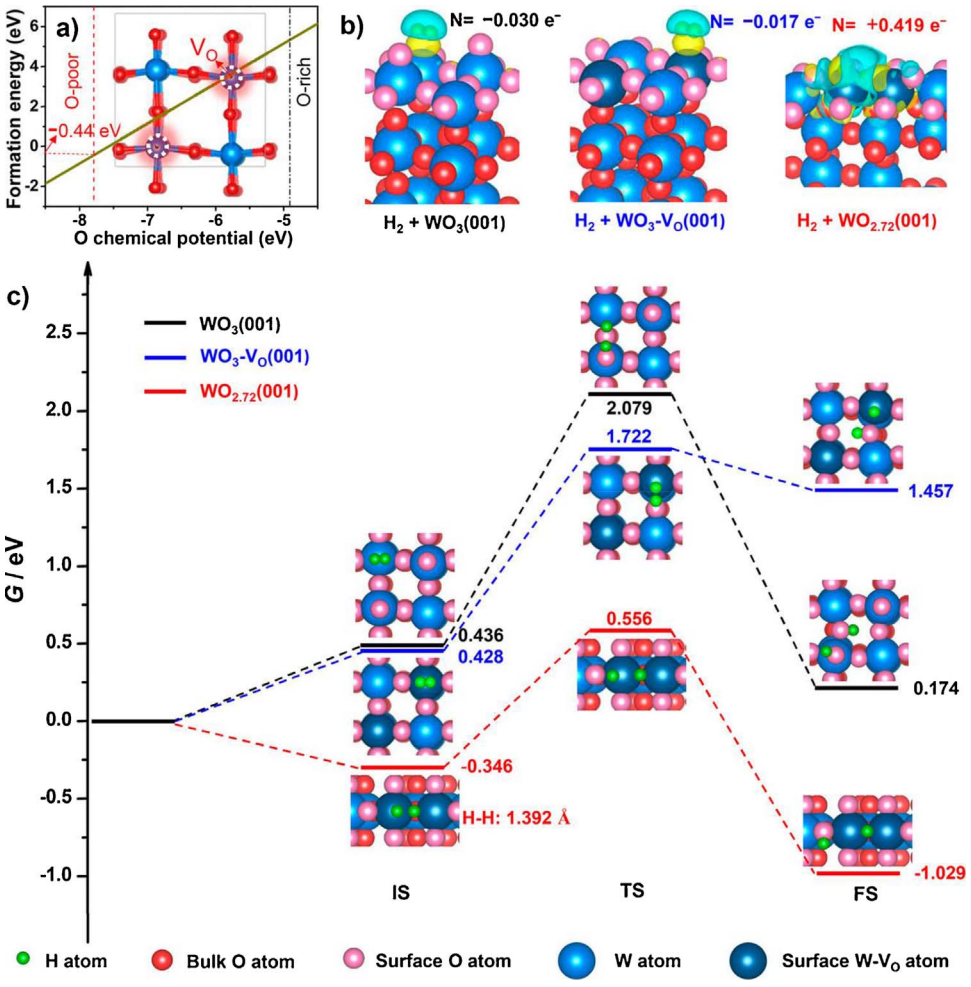

Fig. 3. (a) Formation energy of WO_3-V_O surface under different O chemical potential (T = 0 K). (b) Differential charge density of H_2 adsorption. (The yellow and blue colors represent charge depletion and accumulation, respectively, with iso-surface value of 0.002 e Å^{-3}). (c) Free energies of the initial (IS), transition (TS) and final states (FS) for the dissociation of H_2. (reproduced from Ref. [32] with permission. Copyright 2015, American Chemical Society). (For interpretation of the references to color in this figure legend, the reader is referred to the web version of this article.)

CeO_2 can be explained by preferential adsorption of nitro group on active sites (i.e. oxygen-deficient sites, and edge/corner sites of Au), thereby hindering adsorption and unselective hydrogenation of other groups [5,28]. However, the dissociation of H_2 on reductive support is often difficult compared with the case of metal. Thus, the metal oxide as direct hydrogenation catalyst without the assist of any metal is quite challenging.

Recently, some metal oxides such as WO_x and MoO_x are reported to have metallic feature with the conduction band crossing over the Fermi level [29–31]. As a result, they can function like metal for H—H combination or H_2 dissociation due to the relatively moderate W(Mo)-H binding strength. It is expected that metal oxides with proper modifications can be directly used as promising hydrogenation catalyst. For example, Zou et al. reported the presence of oxygen vacancies in WO_3 can easily promote the activation and dissociation of molecular H_2 using DFT computation [32]. As shown in Fig. 3, on stoichiometric WO_3(001) surface, the adsorption of H_2 is unfavorable and H_2 is almost inactivated. Subsequently, the breaking of H—H bond is kinetically unfeasible (with high barrier of 1.643 eV), with two dissociated H atoms binding with terminal and bridge O atoms respectively. On WO_3-V_O(001) constructed by taking one oxygen atom away from WO_3 surface, the H_2 adsorption free energy and energy barrier for H—H bond cleavage become slightly lower (0.428 eV and 1.294 eV, respectively), indicating a tendency for easier H_2 activation. Notably, the presence of oxygen vacancy changes the way of H_2 dissociation, with one dissociated H atoms binding with surface W atom and the other with bridge O atom. On $WO_{2.72}$(001) surface abudant with oxygen vacancies, H_2 is activated in the same way, but the adsorption of H_2 is very easy (with adsorption free energy of −0.346 eV). Importantly, $WO_{2.72}$(001) surface has a strong interaction with H_2 by transferring 0.419 e$^-$ to H_2, and the H—H bond is elongated to 1.392 Å. As a result, the energy barrier for H—H bond dissociation is only 0.902 eV with considerable exothermic energy of 0.683 eV, indicating the H_2 activation is favorable from the aspect of both kinetics and thermodynamics. They also found that both perfect and oxygen-deficient Co_3O_4 can easily activate H_2 with two-step process through a heterolytic cleavage followed by the transfer of H atom and finally yields the homolytic product [33,34]. Moreover, the activation barriers in both steps are low with only 0.54 and 0.57 eV on these two surfaces. Wu et al. also studied the role of CeO_2 in the hydrogenation reaction, especially the activation of H_2 [35]. They demonstrated the first direct spectroscopy evidence for the presence of both surface and bulk Ce-H species upon H_2 dissociation and pointed out a heterolytic dissociation mechanism involving either homolytic products (surface OHs) on a close-to-stoichiometric CeO_2 surface or heterolytic products (Ce-H and OH) with the presence of induced oxygen vacancies in CeO_2.

3. Catalysts for hydrogenation of nitroarene using H_2

The catalysts that have been explored so far for selective catalytic hydrogenation of nitroarene using H_2 include metal, metal oxide, sulfide/carbides, nitrides and boride, and functional carbon material. In the below sessions, we will review these catalysts by focusing on how to tune structure and composition of catalyst towards high activity and selectivity.

3.1. Metal

Metals such as Pt, Pd, Ru, Ni and Co, are highly active for hydrogenation, but in most cases, cannot discriminate competitive functional groups such as nitro and olefinic groups [36]. Various strategies including the use of metal-support interaction, size effect, single-atom, alloy effect, strain effect, shape-selective catalysis, and interfacial adsorbent-metal interaction are explored to promote the selectivity.

3.1.1. Metal-support interaction

The dissociation of H_2 on metal surface is thermodynamically and kinetically favourable. However, commercially available metals such as Pt and Ni cannot be used to hydrogenate substituted nitrobenzenes with H_2, since they are not selective due to the aforementioned parallel adsorption of nitroarene. With the help of reductive supports such as TiO_2, the selectivity and stability can be improved due to the strong metal-support interaction and optimized adsorption mode of nitro group. For example, Corma et al. reported that by tuning the metal-support interactions, high selectivity (90%–95%) over Pt/TiO_2, Pt/C, Ru/TiO_2 and even Ni/TiO_2 catalysts while maintaining a high activity can be obtained [4]. Recently, Gao et al. used hydrogenated MoO_x (H-MoO_x) to load bimetallic Pt-Sn (Pt-Sn/H-MoO_x) for the selective hydrogenation of 4-nitrostyrene, and obtained an outstanding selectivity to 4-vinylaniline of 93% and high turnover frequency of 0.094 s^{-1} [37]. In addition to reductive metal oxide, some carbon material with oxygen and nitrogen surface groups can also function as adsorption sites for nitro group [38–40]. Motivated by these, Zhang et al. reported the oxygen surface groups (OSGs) of activated carbon can steer the selective hydrogenation of substituted nitroarenes over Ni nanoparticles, by using the strong interaction between OSGs and nitro group as well as the excellent hydrogenation ability of Ni [41]. Xia et al. reported the interaction of Co nanoparticles with nitrogen-functionalized carbon nanotubes (CNTs) via the hybridization of π orbitals of N with d orbitals of Co [42]. They found that surface nitrogen species on CNTs significantly promot the decomposition of the cobalt precursor and the reduction of cobalt oxide, and improve the resistance of metallic Co against oxidation in ambient atmosphere. In the selective hydrogenation of nitrobenzene, Co supported on CNTs with the highest surface nitrogen content shows the highest activity, ascribed to the higher reducibility and the lower oxidation state of the Co nanoparticles under reaction conditions. Coupling the advantages of metal oxide and carbon, Zhang et al. synthesized graphene nanosheet-supported ultrafine Pt nanoparticles encapsulated by thin mesoporous SiO_2 layers (Pt-rGO@mSiO_2) for catalytic hydrogenation of 4-nitrophenol to 4-aminophenol under mild conditions (1 atm H_2 and 25 °C) [43]. Intriguingly, the catalyst gives complete conversion (100%) in 50 min, whereas Pt-rGO(etched) gives a conversion of only 87%, and Pt-rGO shows an even lower conversion of 25%, owing to the larger size and aggregation of Pt nanoparticles. Based on this, they assembled Au-Fe_3O_4 dimers to Au-Fe_3O_4 clusters, and got naked Au-γ-Fe_2O_3 clusters by calcining them using a silica protection/deprotection strategy (Fig. 4a) [44]. Due to their clean surfaces, mesoporous structure, and excellent interfacial contact between Au NPs and γ-Fe_2O_3 NPs, the clusters displayed excellent catalytic performance in the hydrogenation of 4-nitrophenol, whereas other controlled catalysts including individual Au NPs and self-assembled Au-Fe_3O_4 clusters show negligible activities.

3.1.2. Size effect

Various metal coordination sites (terrace, edge, kink, or corner sites) are present on metal nanoparticles [45], which often exhibit quite different capability toward H_2 dissociation due to the distinct surface structure and electronic properties, thus showing different hydrogenation activity [46]. And the distribution of these sites is often dependent on the size of metal nanoparticles. Moreover, the adsorption of nitro group on metal is stronger than that of other functional groups and thus the steric effect induced by smaller size hinds the adsorption of other functional groups and improves the reaction selectivity [22]. Practically, metal nanoparticles are often supported on high surface area materials to prevent their aggregation. For example, Qie et al. reported Ni nanoparticles with the size of 5 nm supported on carbon material by directly heating sheet-like $Ni(OH)_2$-based composites at 300 °C, which exhibits excellent performance for selective hydrogenation of chloronitrobenzene to chloroanilines [47]. Similarly, Figueiredo et al. reported Ni/C catalyst synthesized by decomposing methane over Raney-type skeletal Ni for selective hydrogenation of nitrobenzene [48]. Recently, Kempe et al. reported Ni and Co nanoparticles with diameters of 5.5 and 1.5 nm supported on mesostructure silicon carbonitride (SiCN) to hydrogenate nitroarenes (Fig. 4b, c) [49,50]. The synthetic process follows two-step procedure, in which Ni or Co(II) organometallic complex and polysilazane are dissolved in tetrahydrofuran (THF), followed by crosslinking using dicumylperoxide (DCP) and pyrolyzed under N_2 at 800–900 °C. Both Ni and Co nanoparticles show high activity in the hydrogenation of nitroarenes to anilines, and offer excellent tolerance to reducible groups such as C=C bonds, heteroaromatics, and nitrile, keto, aldehyde, and amide groups. Ni nanoparticles are robustness, recycled and reused over multiple runs without decrease in activity or selectivity. But Co particles show a slight decrease in the activity in the third run and a significant decline in the fourth run (Fig. 4c). However, leaching of Co during the reaction is very low (0.5%), and the activity is easily regained through temperature programmed reduction (TPR) treatment to reduce Co oxide species, indicating the reduced state is very important in the hydrogenation. Also, Raja et al. reported the synthesis of 3 nm Co nanoparticles from colloidal precursors and mesoporous silica supports, for highly effective, recyclable and selective hydrogenation of a range of nitro-substituted aromatics under mild conditions [51].

3.1.3. Single-atom catalyst

The lowest limit of downsizing metal particles is to disperse the metal as exclusively isolated single atoms, called as single-atom catalyst (SAC) [52,53]. It is expected that SAC may have superior performance in selective hydrogenation reactions due to the effective coupling the size effect and metal-support interaction. Zhang et al. reported that FeO_x-supported Pt single-atom and pseudo-single-atom structures are extremely active, selective and recyclable for the hydrogenation of a variety of functionalized nitroarenes (Fig. 5a) [40]. More importantly, characterizations reveal that the pseudo-single-atom structure is composed of a few to tens of atoms loosely and randomly associating with each other but do not form strong Pt-Pt metallic bonding, resembling the structure and function of isolated single atoms. For the selective hydrogenation of 3-nitrostyrene, the turnover frequency (TOF) of SAC and pseudo-SAC reaches as high as ~1500 h^{-1}, 20-fold higher than that of the best catalyst reported in literature (Pt/TiO_2). Furthermore, the selectivity toward 3-aminostyrene is close to 99%, again the best result ever achieved over Pt-group metals. The superior performance can be attributed to the presence of positively charged Pt centres and the absence of Pt-Pt metallic bonding, both of which favour the preferential adsorption of nitro groups. They also reported a self-supporting Co—N—C catalyst wherein Co is dispersed exclusively as single atoms (Fig. 5b, c) [54]. The exact structure is identified as CoN_4C_8-1-$2O_2$, where the Co center atom is coordinated with four pyridinic N atoms in the graphitic layer, while two oxygen molecules are weakly adsorbed on Co atoms perpendicular to the Co-N_4 plane. This Co—N—C catalyst presents excellent performance for the selective hydrogenation of nitroarenes to produce azo compounds under mild conditions. What is of more interest is the unprecedented selectivity for diverse nitroarene substrates, as both electron-rich and electron-deficient nitroarenes are converted quickly into azo products. Moreover, for the more challenging 3-nitrostyrene, the catalyst can hydrogenate the nitro group to azo group without any detectable concurrent hydrogenation of the alkene groups. Both control reaction and attenuated total reflection infrared spectra (ATR-IR) results reveal the alkene group cannot be

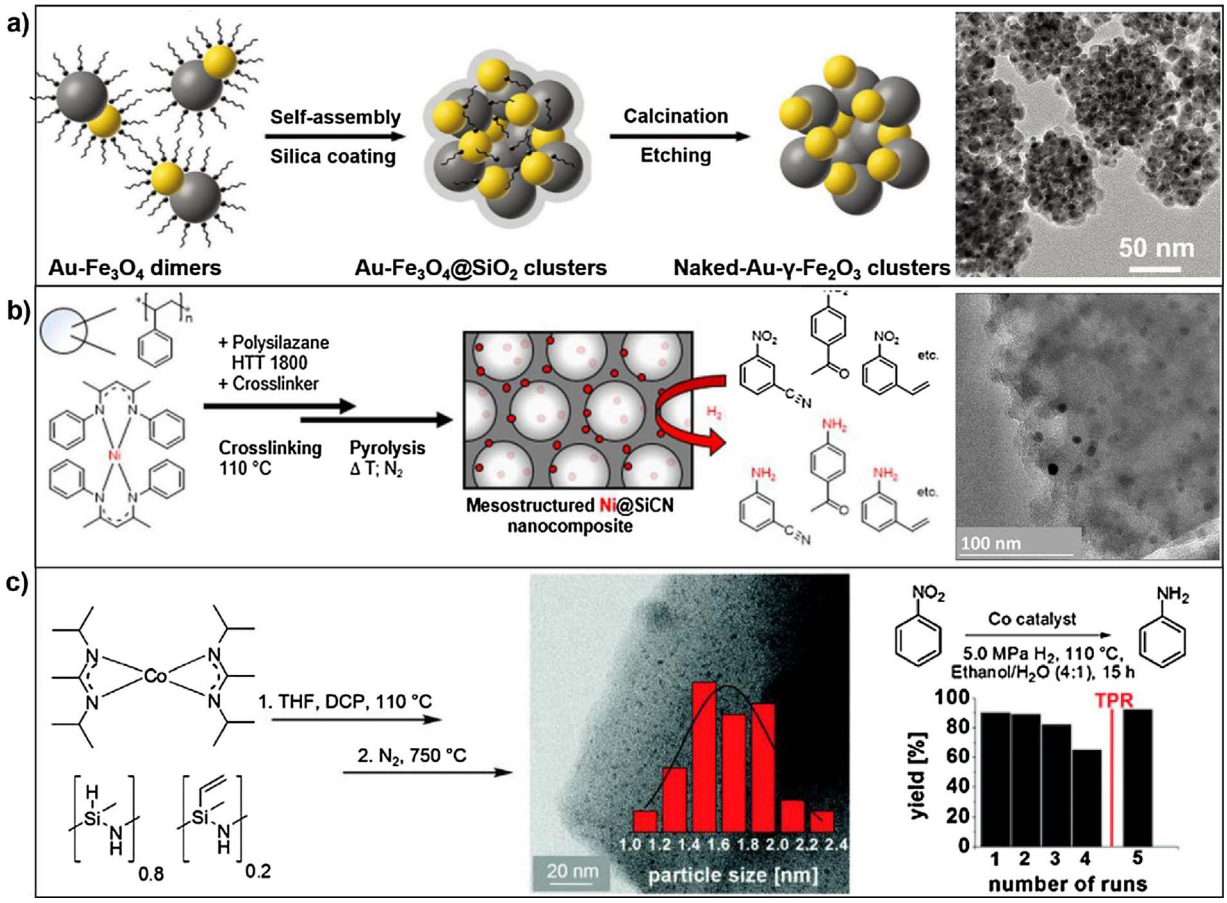

Fig. 4. (a) Synthesis of magnetic mesoporous naked-Au-γ-Fe_2O_3 clusters. (a reproduced from Ref. [44] with permission. Copyright 2017, Wiley Online Library) (b) Synthesis of reusable Ni catalyst supported on mesostructured silicon carbonitride for selective hydrogenation of substituted nitroarenes. (b reproduced from Ref. [49] with permission. Copyright 2016, Wiley Online Library) (c) Synthesis of reusable Co catalyst supported on mesostructured silicon carbonitride for the selective hydrogenation of substituted nitroarenes. (c reproduced from Ref. [50] with permission. Copyright 2016, Wiley Online Library).

adsorbed on the Co—N—C moieties at all, accounting for the extraordinarily high selectivity. Similarly, Su et al. fabricated Co-NC/CNTs and investigated the catalytic performance in nitrobenzene hydrogenation [55]. Catalysts with and without acid treatment present essentially the same activity, suggesting that the CoN_x sites highly dispersed in CNTs formed during pyrolysis, rather than the Co particles, are the real active sites. Recently, Qu et al. reported sub-nanometric Pd clusters supported on porous CeO_2 nanorods with a high surface Ce^{3+} fraction and a large concentration of oxygen vacancy (named as PdsNC/*PN*-CeO_2) (Fig. 5d) [56]. For hydrogenation of 4-nitrophenol, the catalyst shows a high selectivity of > 99.9% toward 4-aminophenol and a large turnover frequency (TOF) of ~44,059 h^{-1} based on exposed Pd atoms. Both experimental and theoretical results suggest that the superior catalytic activity and selectivity are originated from the cooperative effect between the highly dispersed Pd for H_2 dissociation and *PN*-CeO_2 for the highly preferential adsorption of nitroarenes.

The big challenge for single atom catalyst is to increase the loading of active metal components to make the catalysts effective enough for structure characterization of active sites and also for practical applications [53,57]. Possibly, such issue can be counteracted by structural modification of the support with high specific surface area, appropriate porosity, and surface modification with high affinity to anchor single metal atoms. Yan et al. introduced phosphomolybdic acid (PMA) on activated carbon (AC) to stabilize single Pt atom with 1.0 wt% loading [58]. With 36 oxygen atoms exposed, PMA furnishes a range of coordination sites including single corner site, bridge site (the O_c-O_{br}-bridge site), three-fold hollow site (3-H_O_c and 3-H_O_{br}), and four-fold hollow site (4-H) (Fig. 6a). XAS and DFT results (Fig. 6b–e) confirm Pt atom interacts with four bridging oxygen atoms and form a relatively stable structure in the 4-H site. As a result, Pt species in Pt-PMA/AC are positively charged by electron transfer from Pt to PMA, and absorbs hydrogen easily as confirmed by H_2-O_2 titration experiment. For hydrogenation of nitrobenezene, aniline is the only product obtained over Pt-PMA/AC, whereas five different products are detected for Pt/AC, including aniline, nitrosobenzene, phenylhydroxylamine, azobenzene, and azoxybenzene with overall selectivity of only 50% towards aniline (Fig. 6f). Considering that the side products are all intermediates in nitrobenzene hydrogenation, the exceptional selectivity may, at least partially, be due to the presence of Pt single atoms on Pt-PMA/AC, which adsorb and polarize the intermediates and transform them into aniline.

Recently, Zheng et al. developed a photochemical strategy to prepare highly stable atomically dispersed Pd catalyst with loading over 1.5 wt% on ultrathin ethylene glycolate (EG)-functionalized TiO_2 nanosheets (Pd1/TiO_2) [57]. Pd centers are square-planarly coordinated by four oxygen atoms (two from EG fixed on Ti, one from unbound O on EG, and one from coordinated H_2O). With such unique Pd-EG-TiO_2 coordination interface, the Pd centers activate H_2 via heterolytic splitting. According to DFT calculations, H_2 adsorbed on Pd atom is readily split into two H atoms, with one H atoms moving to nearby oxygen on EG to yield O-$H^{\delta+}$ and leaving the other H atom on Pd as $H^{\delta-}$. Although the authors didn't test nitroarenes hydrogenation, the catalyst exhibits high catalytic activity in hydrogenation of C=O bonds, similar to nitro group of nitroarenes. Therefore, these structures can bring opportunities to stimulate the synthesis of SACs for nitroarenes hydrogenation.

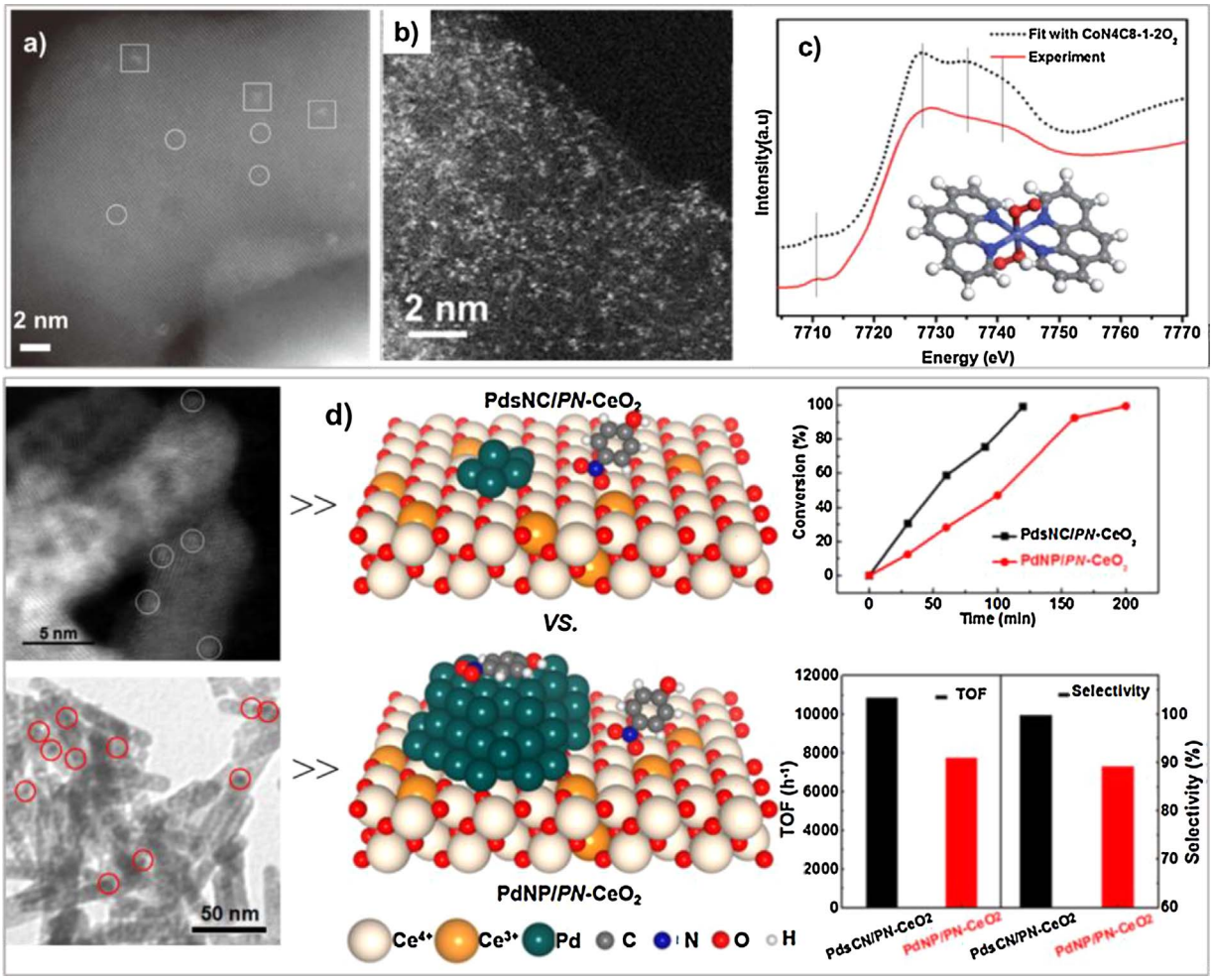

Fig. 5. (a) TEM image of FeO_x-supported platinum single-atom catalysts. (a reproduced from Ref. [40] with permission. Copyright 2014, Nature Publishing Group) (b, c) Morphology and structure identification of single-atom Co—N—C catalyst. (b, c reproduced from Ref. [52] with permission. Copyright 2016, Royal Society of Chemistry) (d) Sub-nanometric Pd clusters on porous nanorods of CeO_2 for hydrogenation of nitroarenes. (d reproduced from Ref. [56] with permission. Copyright 2016, American Chemical Society).

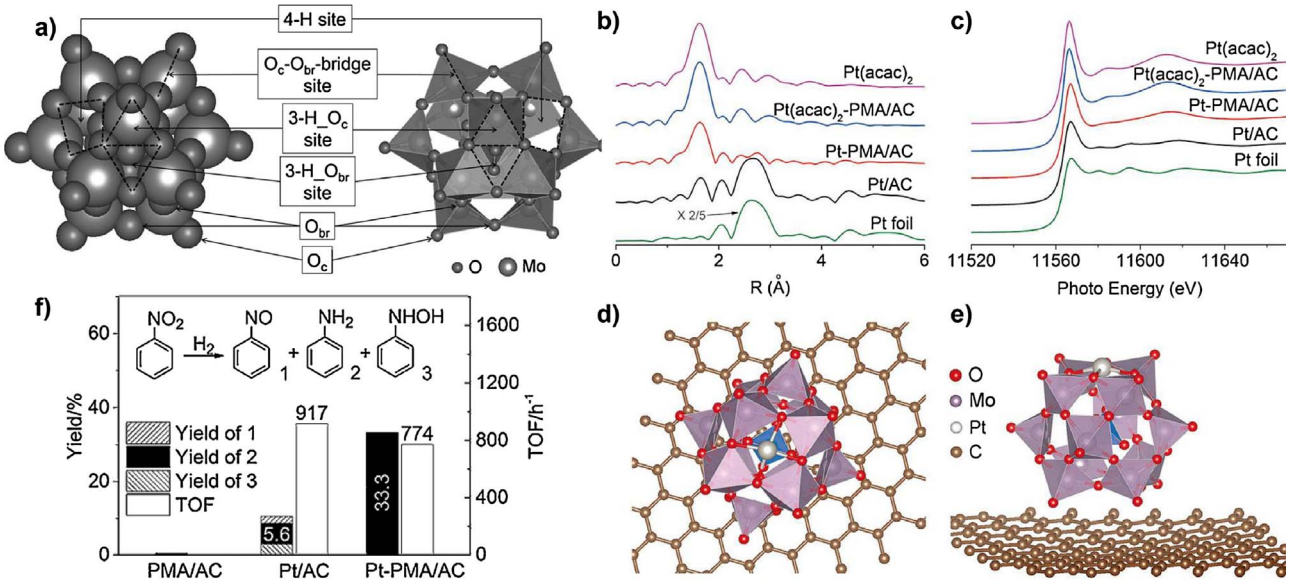

Fig. 6. (a) Different types of surface O atoms and possible anchoring sites for Pt atoms on Keggin-structured anion phosphomolybdic acid ($PMo_{12}O_{40}^{3-}$). (b, c) EXAFS and XANES spectra at Pt L3-edge of Pt-based catalysts. (d, e) Most stable configuration of Pt_1 on PMA/graphene, based on DFT calculations. (f) Catalytic performance of PMA/AC, Pt/AC, and Pt-PMA/AC in hydrogenation of nitrobenzene. (reproduced from Ref. [58] with permission. Copyright 2016, Wiley Online Library).

3.1.4. Alloy and strain effect

Au is highly selective for nitroarenes hydrogenation but hindered by the limited H_2 dissociation dynamics, whereas other metals such as Pt and Pd can dissociate H_2 readily [59], thus TiO_2-supported bimetallic Pt-Au and Pd-Au can be used to improve the selective hydrogenation of nitroarenes [26,60]. Actually, the formation of alloy can also induce the compressed or expanded arrangements of surface atoms to alter the crystal lattice strain [61,62]. Recent reports demonstrated that the catalytic activity could be influenced by tuning the lattice strain of metal catalysts because the lattice strain can modify the electronic structure of catalysts and further affect the adsorption of reactants, and corresponding activation barrier of transition-state [63–67]. In this regard, tuning the lattice strain of metal catalysts might be a new effective strategy to control the catalytic selectivity. Recently, Li et al. reported the selective hydrogenation of 4-nitrostyrene using dumbbell-shaped Co-Ru nanostructure composed of a Co nanorod with two ends capped with Ru nanoplates [64]. The crystal lattice of Ru at both ends is compressed due to the connection of Co at the center compared to pristine Ru. As a result, Ru and $Co_{0.46}$-$Ru_{0.54}$ NPs produced comparable 4-nitroethylbenzene to 4-aminostyrene; $Co_{0.12}$-$Ru_{0.88}$ and $Co_{0.38}$-$Ru_{0.62}$ gave relative lower selectivity of 4-nitroethylbenzene. Notably, almost no 4-nitroethylbenzene was found using $Co_{0.23}$-$Ru_{0.77}$ as a catalyst, indicating its specific hydrogenation selectivity on $-NO_2$ group. Interestingly, the selectivity of 4-aminostyrene is in a volcano-type fashion with the compressive lattice strain of Ru. Pristine Ru gave only 66% selectivity, and the selectivity was increased to 99% when compressing the Ru lattice strain with 3% (from pristine 2.14 to 2.08 Å); however, decreased selectivity was found when further increasing the compressive lattice strain gradually. DFT computation demonstrated that the optimized lateral compressive strain (3%) facilitates hydrogenation of $-NO_2$ group but impedes hydrogenation of $-C{=}C$ group. Additionally, the strained $Co_{0.23}$-$Ru_{0.77}$ catalysts could be easily recycled for at least 4 times without obvious loss of activity and selectivity.

3.1.5. Shape-selective catalysis

Zeolites, which have been widely applied in petrochemical industry, are well-known for shape-selective catalysis [68], whereby the molecules are adsorbed in a sterically controlled fashion and selectively transformed to target product in the uniform micropores, thus giving unusual selectivity in various reactions. Recently, Xiao et al. reported a method for selective hydrogenation of substituted nitroarenes like 4-nitrochlorobenzene and 4-nitrobenzaldehyde using metal@zeolite core-shell catalysts that combine the advantages of metal nanoparticles (high catalytic activities) and zeolite micropores (selective adsorption of reactants) (Fig. 7) [69]. In contrast, conventional supported catalysts such as Pd/C and Pd/Beta are nonselective and lack stability. In competitive adsorption experiments with mixture of chlorobenzene and nitrobenzene, IR spectrum of Pd@Beta shows only the bands of nitro group (1529 and 1362 cm^{-1}), indicating the selective adsorption of nitrobenzene. Similar results were obtained in competitive adsorption tests with mixture of benzaldehyde and nitrobenzene. All these results demonstrate a unique feature of Pd@Beta for selective adsorption of nitrobenzene and account for the superior selectivity of the catalyst in hydrogenation of nitroarenes (Fig. 7c). Pd leaching is a general problem for many supported catalysts, and their stability and recyclability are critical for industrial application. However, Pd@Beta shows stable performance in recycling tests, and Pd leaching or aggregation is not detected in long-term flow test. The reason is that the particle size of Pd is larger than the micropore diameters of zeolite Beta, which is beneficial for fixing Pd nanoparticles within the zeolite framework.

3.1.6. Interfacial adsorbate-metal interaction

The application of organic/inorganic adsorbate to modify the electronic properties of active metal has recently been suggested [70–72]. Recently, Zheng et al. synthesized ethylenediamine (EDA)-coated ultrathin Pt nanowires (EDA-Pt NWs) and demonstrated that organic

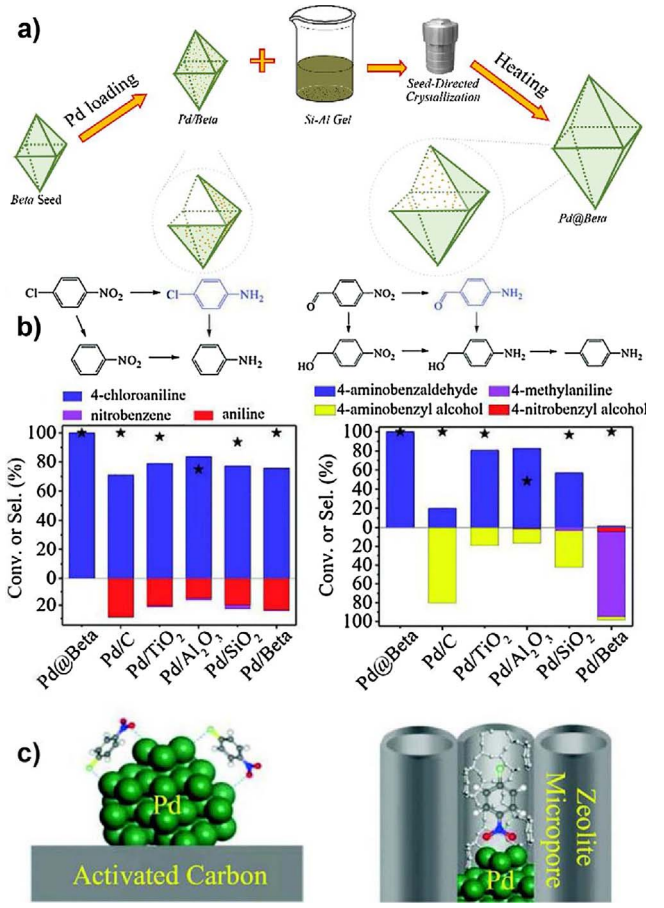

Fig. 7. (a) Synthesis strategy of the Pd@Beta. The dotted-line cycles highlighted section view of the Pd/Beta and Pd@Beta. (b) Substrate conversions (★) and product selectivities (colored columns) for the hydrogenation of 4-nitrochlorobenzene and 4-nitrobenzaldehyde on various catalysts. (c) Proposed models for the adsorption of 4-nitrochlorobenzene on Pd/C and Pd@Beta. (reproduced from Ref. [69] with permission. Copyright 2017, Wiley Online Library).

adsorbate on metal surface readily induces a perfect interfacial electronic effect to shape the catalytic selectivity [25,45]. The catalyst exhibit unexpectedly high selectivity for the production of phenylhydroxylamine, a thermodynamically unfavorable but industrially important chemical. The selectivity is nearly 100% at the full conversion of nitrobenzene at 50 min, and well maintained even when the reaction time is prolonged to 2 h. Such a high selectivity cannot be achieved by pristine Pt. DFT calculations reveal that the electron donation from EDA makes Pt highly electron rich, thus favoring the adsorption of electron-deficient reactants over electron-rich substrates like phenylhydroxylamine and preventing it being full hydrogenated to anilines.

3.2. Metal oxide

Metal oxides typically serve as support to load active metal sites to control the overall hydrogenation performance including the selectivity and reaction rate [3,5]. For example, the hydrogenation of nitrobenzene over Au/TiO_2 proceeds through the direct route, whereas Au/CeO_2 proceeds through the condensation route [28,73]. For the condensation route, a high nitrosobenzene concentration is necessary. In the case of Au/TiO_2, nitrosobenzene is rapidly converted into phenylhydroxylamine, which accumulates on the surface and is then transformed to aniline. The concentration of nitrosobenzene is never high enough to form azoxybenzene. For Au/CeO_2, the rate of hydrogenation is considerably lower, and the conversion of nitrobenzene and

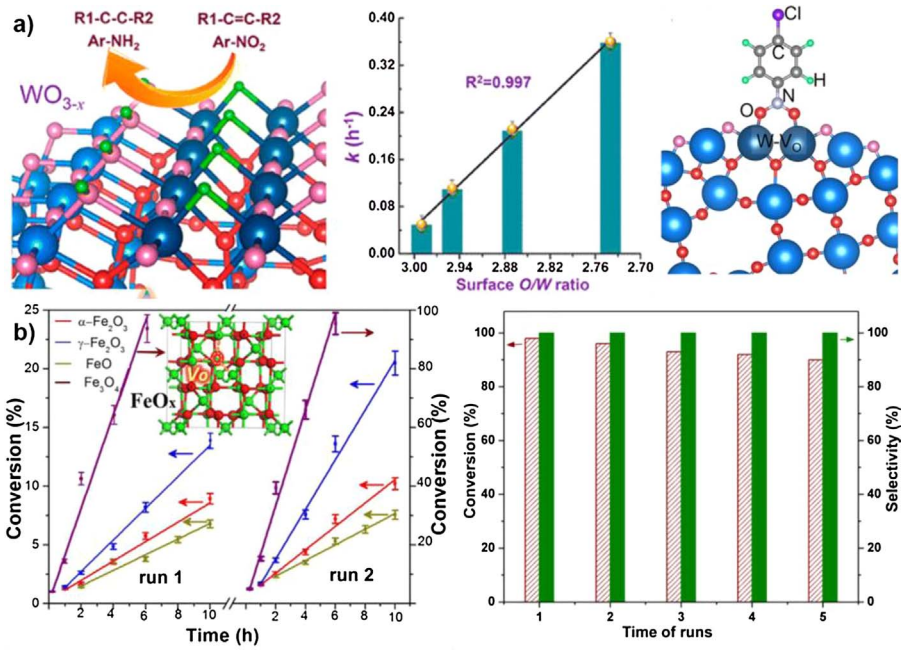

Fig. 8. (a) Oxygen-deficient tungsten Oxide as efficient hydrogenation catalyst. (a reproduced from Ref. [32] with permission. Copyright 2015, American Chemical Society) (b) Iron oxide as catalyst for nitroarenes hydrogenation: the important role of oxygen vacancies. (b reproduced from Ref. [75] with permission. Copyright 2016, American Chemical Society).

nitrosobenzene are slower; as a result, nitrosobenzene can accumulate and form condensation intermediates. But all these catalysts need the active metal phase such as Au and Au-Pt alloy for H_2 dissociation. Recently, some oxygen-deficient and N-doped metal oxides and have been reported to show the capability for H_2 dissociation [7,9,32].

3.2.1. Defect engineering

Defect engineering can enhance the electron transfer from defect site to metal d band to further tune H_2 activation and dissociation [74–77]. Moreover, oxygen-deficient metal oxide can easily adsorb nitroarene like the case in Au/TiO_2 catalsyst [3,5]. Thus, they can function as efficient catalyst for selective hydrogenation of nitroarene. Taking WO_x family as example, it is one of the most-attractive reductive metal oxides with the nonstoichiometric property, providing promising active site for the adsorption of nitroarene and molecular H_2 dissociation. Zou et al. reported the presence of oxygen vacancies help to activate molecular H_2 and therefore tuning the oxygen vacancies may make inert oxides become active hydrogenation catalyst (Fig. 8a) [32]. Interestingly, the initial reaction rate is linearly dependent on the surface O/W ratio with very good correlation coefficient of 0.997, the lower the ratio, the quicker the reaction proceeds. $WO_{2.72}$, as the extreme oxygen-deficient oxides, having stable crystal phase (not just surface reduced WO_3), gives 100% selectivity for substituted anilines and keep other functional groups such as chloride, formyl and carboxyl groups un-affected, whereas Ni leads to much lower selectivity because the substituted groups or aromatic rings are hydrogenated. The perfect selectivity of $WO_{2.72}$ is attributed to the distinct adsorption mode. $WO_{2.72}$ captures oxygen atom of $-NO_2$ preferentially to fill the oxygen vacancy, and more importantly, nitro group is vertically adsorbed onto $WO_{2.72}$(001) surface, with other groups away from the catalyst surface to avoid further activation and hydrogenation. Moreover, $WO_{2.72}$ shows very stable conversion and selectivity in recycling experiment, indicating the occupied oxygen vacancies can be fully recovered in the catalytic circle.

Also, Zou et al. reported iron oxide as catalyst for nitroarene hydrogenation (Fig. 8b) [77]. It is found that γ-Fe_2O_3, α-Fe_2O_3, and FeO (with similar structure and surface area) show obvious but a little limited activity, but the activity of the used catalyst is increased in the second run, especially for γ-Fe_2O_3. Characterization shows that Fe_2O_3 is partly reduced with many oxygen vacancies produced on the surface, which accounts for the hydrogenation activity. Finally, Fe_3O_4 exhibits activity significantly higher than Fe_2O_3 and FeO, and 100% selectivity in the hydrogenation of nitroarenes to anilines. Also, Fe_3O_4 is easy to separate by a magnetic field and shows excellent recycling stability. Overall the report on individual metal oxide as nitroarene hydrogenation catalyst is very limited. However, oxygen-deficient metal oxides including CeO_{2-x} [78,79], In_2O_{3-x} [80,81], MoO_{3-x} [82] have been reported as catalyst for CO_2 hydrogenation, semihydrogenation of acetylene and so on. It is expected that these catalysts can bring more opportunities for nitroarenes hydrogenation.

3.2.2. Metal oxide/N-doped carbon interaction

Similar to metal-support interaction, the coupling of metal oxide with N-doped carbon material are promising as hydrogenation catalyst, because the interaction of N species with metal centre produces new active sites. Beller et al. reported inexpensive Co-based metal oxide catalyst derived from the pyrolysis of Co phenanthroline complexes at higher temperatures (800 °C) for 2 h under inert gas atmosphere (Fig. 9a), composed of nanoscale Co_3O_4 nanoparticles surrounded by N-doped graphene layers (Fig. 9b) [7]. This catalyst is applied to the hydrogenation of a wide range of nitroarene substrates under a hydrogen pressure of 50 bar in aqueous THF at 110 °C to afford anilines in excellent yields with excellent selectivity (Fig. 9c, d). Using the same method, other metal oxide such as Fe_2O_3 and NiO are also synthesized [9,83–86]. Especially, Fe_2O_3-based catalyst facilitate the hydrogenation of numerous structurally diverse nitroarenes (more than 80 examples) in good to excellent yield under industrially viable conditions [9]. Comparison of characterization and catalytic results suggests that it is these particular FeN_x centers formed in a narrow range of pyrolysis temperatures around 800 °C that govern the unique catalytic activity, and the size of Fe_2O_3 particles seems to play a minor role as long as their growth does not reduce the exposed active surface. Similarly, they synthesized Co-based hydrogenation catalyst by the assembly of cobaltdiamine-dicarboxylic acid metal organic frameworks on carbon and subsequent pyrolysis under inert atmosphere [87].

3.3. Metal sulfide/carbides, nitrides and boride

Metal sulfide/carbides, nitrides and boride have been widely reported for traditional hydrodesulphurization technology due to their suitable H adsorption for hydrogen dissociation [1]. They are also studied as catalyst for nitroarenes hydrogenation. For example, Zhang

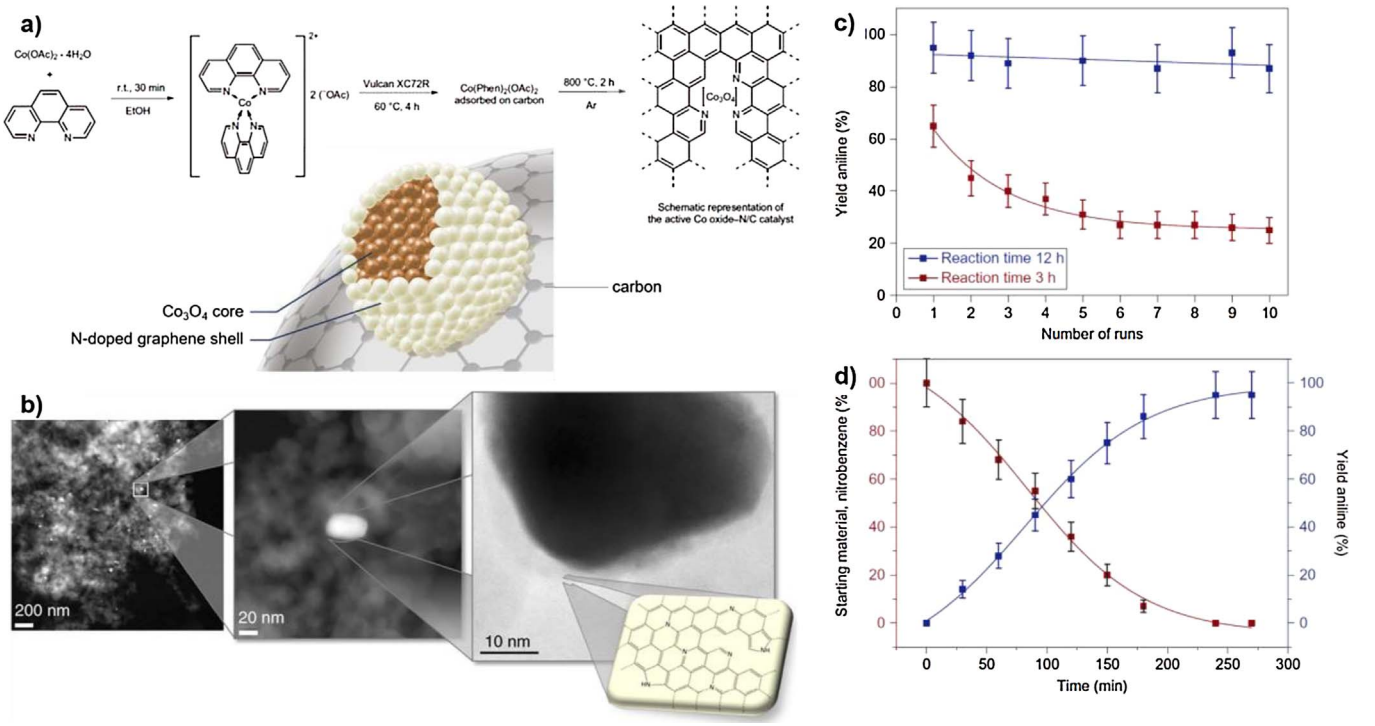

Fig. 9. Pyrolysis of Co phenanthroline complexes to produce Co_3O_4 particles surrounded by N-doped graphene layers for hydrogenation of nitroarenes. (reproduced from Ref. [7] with permission. Copyright 2013, Nature Publishing Group).

et al. reported Ni_7S_6 nanostructures for selective hydrogenation of chloronitrobezene, and the flowerlike morphology is more active than the others [88]. The conversion order of the nitroarenes over flowerlike Ni_7S_6 is: *o*-chloronitrobenzene > *m*-chloronitrobenzene > *p*-chloronitrobenzene > nitrobenzene. The presence of electron-withdrawing group −Cl results in higher activity than nitrobenzene due to the enhanced adsorption strength of $-NO_2$ on catalyst surface [89].

Keane et al. reported ternary nitride catalysts for nitroarenes hydrogenation [90]. They found that Fe_3Mo_3N selective hydrogenates $-NO_2$ in *p*-chloronitrobenzene to generate *p*-chloroaniline as sole product, whereas Co_3Mo_3N favours C−Cl scission with the formation of nitrobenzene (in addition to *p*-chloroaniline). Hydrodechlorination ability is further confirmed for Co_3Mo_3N in the conversion of chlorobenzene (to benzene) under conditions where Fe_3Mo_3N is totally inactive. A temporal deactivation of both nitrides is associated with Cl poisoning of Co_3Mo_3N and structural changes to Fe_3Mo_3N. Additionally, Ding et al. reported that transition metal-boron alloy (FeB, NiB and CoB) nanotubes are highly active for the hydrogenation of nitrobenzene [91]. They further synthesized high quality ternary NiPB nanotubes with controllable diameters, which possess higher stability than the binary counterparts such as NiB alloys and exhibit superior performance in hydrogenation of *p*-chloronitrobenzene [92]. Noteworthy, the activity of nanotubes is found to increases as their diameter reduces. Also, Li et al. reported the synthesis of spherical Ni-B amorphous alloy through self-assembly of an ionic surfactant hexadecyltrimethylammonium bromide, which exhibits higher activity and selectivity than the regular Ni-B obtained via direct chemical reduction, apparently owing to the high dispersion of active sites and the mesoporous channels [93].

Coupling metal with metal sulfide/carbides, nitrides and boride can obtain improved activity due to the synergistic effect via the optimization of H_2 dissociation and reactant adsorption [1]. For example, Zhao et al. demonstrated that Ni-W_2C supported on activated carbon (AC) or mpg-C_3N_4 is promising catalyst for selective hydrogenation of diverse nitroarenes to anilines, exhibiting higher activity than the two individuals [94]. The result also challenges the long-held axiom that the combination of Lewis acid and hydrogenation catalyst mainly enhances the transformation of nitrobenzene to *p*-aminophenol via Bamberger rearrangement of phenylhydroxylamine (PHA) intermediate.

3.4. Functional carbon material

Carbon is inert in hydrogenation because its interaction with adsorbed species (such as H_2 and $-NO_2$ group) is very weak due to the uniform charge distribution. Doping nonmetal heteroatom such as N, P, S or B in carbon matrix can cause the charge delocalization and thus possibly modulate its electronic structure into metal-like, which helps to afford remarkable catalytic activity in a similar way of metal-based catalysts [61]. Among them, N-doped carbon (CN) are one of the most investigated, which can be prepared through calcination of small organic molecules such as cyanamide, melamine and N-containing polymers, which are widely used as adsorbents for nitroarenes from waste water [95]. Also, they have been considered as outstanding candidates for catalyst support due to the high surface area, well-defined porosity and excellent ligand capability [96,97]. Here, we mainly focus on tuning the carbon materials from inert to active for H_2 dissociation via doping and interfacial electronic effect, and thus they can be directly used as catalyst for nitroarenes hydrogenation.

3.4.1. Heteroatom doping

Heteroatom doping often brings up new defects in nearby sites due to the different coordination, bond length and atomic size between the dopant and carbon atoms, which leads to local charge enrichment around the defect sites beneficial for H_2 dissociation. For example, Zou et al. recently reported the P-doped and lattice-defective carbon as metal-like catalyst for selective hydrogenation of nitroarenes [98]. From DFT computation, the combination of P dopant and lattice defect in carbon can cause significant electron delocalization and change the band structure as metal-like one, and thus both H_2 and nitro group are easily activated for selective hydrogenation. In detail, the targeted carbon catalyst with tunable concentration of P-dopant and lattice defect was fabricated by polymerization and carbonization of phytic acid.

As a result, the optimized catalyst exhibits superior catalytic activity, perfect selectivity and stability in the hydrogenation of nitroarenes, outperforming the reported metal-free, metal-oxide and nickel catalysts. Experiment results further confirmed that the hydrogenation activity is linearly dependent on the P-doping and/or defect concentration.

3.4.2. Interfacial electronic effect

Ding et al. firstly reported the synthesis of CN with encapsulation of Ni for the hydrogenation of nitroarenes to anilines [95]. The whole synthetic process can be summarized as three steps: synthesis of Al_2O_3 nanorod as support; impregnation of Al_2O_3 in $Ni(NO_3)_2$ solution and subsequent calcination to obtain NiO/Al_2O_3; and in-situ encapsulation of NiO/Al_2O_3 with CN to get $CN/Ni/Al_2O_3$. The key role of Ni in the composite is to endow electron to CN; thus, CN is negatively charged and capable for H_2 adsorption and activation. As a result, the interfacial electron effect makes CN from inert to active, and Ni is physically isolated from the reaction environment by CN apart from the common corrosion or poisoning phenomenon. Therefore, the catalyst can perform stably and actively for the hydrogenation of nitroarenes under acidic conditions. In detail, the catalyst shows high performance for the one-step synthesis of *p*-amoniophenol from hydrogenation of nitrobenzene in 15 wt% sulfuric acid. Similarly, Ding et al. further reported an efficient catalyst synthesized in one-step without additional supports or CN precursor, by using an N-containing porous polymer (GTP) [99]. In detail, the process is achieved via dipping $Ni(NO_3)_2$ solution into the polymer, followed by calcination in Ar atmosphere. The magnetic nanocomposite shows good catalytic activity for the hydrogenation of nitrobenzene to *p*-aminophenol and, moreover, maintains the activity when pretreated in 15 wt% sulphuric acid solutions at 393 K for ~100 h, indicating an excellent acidic stability. Recently, Wang et al. reported the interfacial electronic effect between Co and N-doped carbon nanotubes (NCNTs) can decrease the dissociation energies of H_2, enabling carbon shell in the hybrid to activate H_2 [100]. The hybrid is fabricated via thermal condensation of D-glucosamine hydrochloride, melamine, and $Co(NO_3)_2{\cdot}6H_2O$, in which the abundant N species from melamine can provide more surface nucleation sites, allowing efficient anchoring of metal NPs. As a result, the hybrids exhibit excellent catalytic activity and perfect selectivity (> 99%) for a wide range of substituted nitroarenes (21 examples) under relatively mild conditions. Additionally, there is no significant formation of nitroso or polymerized products, which suggests that the reaction may involve the direct hydrogenation of nitrobenzene to aniline.

3.4.3. Special carbon material: fullerene

The rich polytypes of carbon, which include fullerene, nanodiamond, carbon nanotube, and graphene, present a rich class of solid-state materials that are non-polluting and reusable [101,102]. Xu et al. found fullerene can activate molecular H_2 as a novel non-metal hydrogenation catalyst [103,104]. The hydrogenation of nitroarenes to anilines is achieved on this catalyst with high conversion and selectivity under 1 atmospheric pressure of H_2 and light irradiation at room temperature, or under conditions of 120–160 °C and 4–5 MPa H_2 pressure without light irradiation, which is comparable to the case with noble metal catalyst. The reaction mechanism may involve a synergistic exciplex (under light irradiation) or an active complex (under dark conditions). This work opens a door for more effective all carbon molecular-based nonmetal catalyst systems for molecular hydrogen activation.

4. Catalysts for transfer hydrogenation of nitroarenes using hydrogen donor

Catalytic transfer hydrogenation (CTH) offers an alternative for catalytic hydrogenation using H_2 [105–107], by using inorganic hydrazine and $NaBH_4$, and organic formic acid and alcohol, as hydrogen donors in the reduction of chemical bonds. It alleviates the safety concern of handling high-pressure, flammable hydrogen gas, enhances the solubility of hydrogen donor in liquid-phase reactions, and substantially reduces the complexity of the synthesis. Furthermore, the lower hydrogenating capability of most organic hydrogen donors, in comparison to H_2, enhances the degree of control in selective hydrogenation, especially when partially hydrogenated molecules are targeted. Typical catalysts used in catalytic transfer hydrogenation are not strict to that of direct catalytic hydrogenation using H_2, because the formation of active hydrogen species from these hydrogen donors is much easier than the case of H_2 dissociation. For example, individual N-doped carbon can catalyses the transfer hydrogenation of nitroarenes, but cannot be used as catalyst in hydrogen by H_2 [100,108]. These catalysts abstracts H from the hydrogen donor and stabilizes it on the surface, restricting active H* recombination, and then the active hydrogen species can be transferred to nitroarenes (which function as oxidant to clean the adsorbed hydride).

4.1. Catalyst for hydrazine donor

Hydrazine hydrate ($N_2H_4{\cdot}H_2O$) as a promising and stable hydrogen storage compound, is a very suitable reagent for the hydrogenation of nitroarenes, as it generates only N_2 as by-product. Two important issues in transfer hydrogenation of nitroarenes are the activation of nitro group and formation of active hydrogen species from $N_2H_4{\cdot}H_2O$ by breaking N—H bond.

The transfer hydrogenation of nitroarenes employing $N_2H_4{\cdot}H_2O$ has been reported with the use of solid catalysts, such as molybdenum carbide, iron oxides, ceria, and functional carbon materials [108–116]. For example, Guo et al. reported selective hydrogenation of nitroarenes containing sensitive substituents by using supported cobalt-doped molybdenum carbide (Co-Mo_2C/AC, AC is activated carbon modified by H_2O_2 oxidation) as noble-metal-free catalyst [109]. The synergistic effect between Co and Mo_2C allows the catalyst to exhibit unexpected catalytic performance in this transformation. 100% conversion of various substrates with 100% selectivity of functionalized anilines has been achieved, which is comparable to the results for noble metal catalysts. Kappe et al. combined $N_2H_4{\cdot}H_2O$ with rapid in-situ generation of Fe_3O_4 catalyst for transfer hydrogenation of nitroarenes [110]. The use of 0.25 mol% of Fe source and processing time of only a few minutes makes this method extremely valuable both on a laboratory scale and industrial scale, by applying continuous-flow processing. Tang et al. reported Co-doped Fe_3O_4 nanoparticles exhibiting high catalytic efficiency and excellent recyclability in the hydrogenation of chloronitrobenzene using $N_2H_4{\cdot}H_2O$ as donor [111]. Figueras et al. reported Mg-Fe hydrotalcite for the transfer hydrogenation of nitroarenes with $N_2H_4{\cdot}H_2O$ [112]. From Mössbauer spectroscopy the catalyst appears as a well-dispersed ferrihydrite phase supported by MgFeO matrix, and only Fe^{3+} ions can be reversibly reduced by $N_2H_4{\cdot}H_2O$ and reoxidized by nitroarene. This observation and the slope of Hammett plot suggest the catalytic mechanism is similar to that reported for iron oxides [110]. The activity is proportional to the fractional of surface iron oxide, and at equal surface area MgFe oxides are more active than iron oxides.

As aforementioned, nitro groups can be easily adsorbed on basic or reducible supports. Ceria is one focus of investigations due to its unique dynamically reversible Ce^{3+}/Ce^{4+} redox pair, which may lead a strong interaction between CeO_2 surface and nitro groups [55,114]. Yu et al. fabricated various CeO_2 nanorods with well-defined surface planes for the hydrogenation of nitroarene with $N_2H_4{\cdot}H_2O$ as hydrogen donor [114]. They found that CeO_2 nanorods containing [110] plane can efficiently and selectively catalyze the hydrogenation of nitroarene, while CeO_2 with [100] or [111] plane shows poor performance for the reaction. The reaction chemistry is determined by the redox properties of ceria surface as well as the coordinative unsaturation of Ce cations, that is, the rods mainly exposed [110] surface have higher concentration of

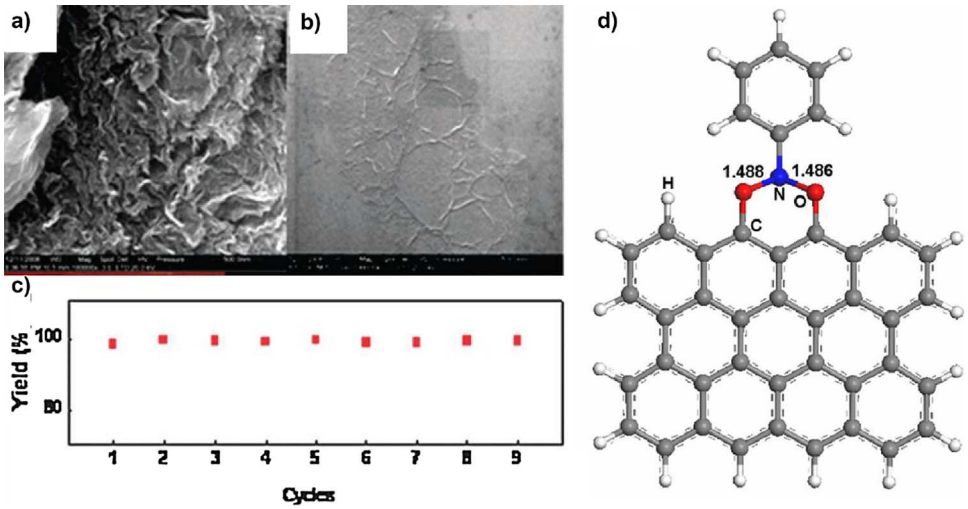

Fig. 10. (a) SEM image of RGO aggregates after filtration and vacuum drying. (b) SEM image of a single RGO sheet laying over Si wafer. (c) Recycling of RGO catalyst for hydrogenation of nitrobenzene. (d) Optimized structure of nitrobenzene molecule reacting with one-layer graphene through two C−O bonds. (reproduced from Ref. [108] with permission. Copyright 2011, Royal Society of Chemistry).

coordinative unsaturated sites than the cubes and octahedra.

Carbon materials, including amorphous carbon, ordered mesoporous carbon, graphite/graphene (oxide) and carbon nanotubes, are widely applied in many transfer hydrogenation of nitroarenes with $N_2H_4{\cdot}H_2O$ donor [117]. For example, Bao et al. reported reduced graphene oxide (RGO) as catalyst for the hydrogenation of nitrobenzene with N-phenylhydroxylamine as intermediate at room temperature (Fig. 10) [108]. High catalytic activity and stability are obtained in cycling experiments. DFT calculations confirm that the zigzag edges of RGO act as active sites to facilitate the activation of reactant molecule. Additionally, when the number of RGO layers decreases, the activation of nitrobenzene becomes easier. Shi and Su et al. also reported O-rich carbon materials as active catalyst in nitrobenzene hydeogenation [115,116]. They demonstrated that the C═O group may be the active site, while a high surface area is also important for achieving high activity. Arai et al. reported an N and O co-doped metal-free carbon catalyst for selective transfer hydrogenation of nitrobenzene and 3-nitrostyrene, which exhibits higher activity than the parent carbon catalyst [118]. They found that the functionalized carbon likely facilitate the adsorption and activation of nitro group through interactions with polarized surface induced by the oxygen and nitrogen hetero dopants.

Many researches are focused on the adsorption and activation of nitroarenes, however, the formation of active hydrogen species from $N_2H_4{\cdot}H_2O$ is very poorly understood [119]. The understanding of $N_2H_4{\cdot}H_2O$ decomposition is mainly obtained from a high-temperature reaction where hydrazine is used as a propellant to generate H_2 [120]. The redox character of central metal plays a crucial role in generating and stabilizing the hydride and proton species. MoO_2 show very special bifunctional metallic-basic properties for metal oxides [29,121]. Its metallicity is attributed to the high density of delocalized electrons in the valence band at the Fermi level, associated with the distorted [MoO_6] octahedral unit [29], which exhibits metallic behavior and can abstract H and stabilize it as a hydride (H^-) species. Its basicity arises from the surface O of Mo-O bonds, which accept H as protons (H^+). Based on these, Wang et al. investigated the formation of active hydrogen species from $N_2H_4{\cdot}H_2O$ catalyzed by MoO_2 and the subsequent transfer hydrogenation of nitroarenes, and suggested multiple Mo atoms as the active sites for hydrazine activation and transfer hydrogenation of nitrobenzene (Fig. 11) [119]. It roughly contains five steps. Step 1: MoO_2 surface with coordination unsaturated Mo sites and basic sites adsorbs N_2H_4 to form adsorbed proton (Mo-OH, $H^{\delta+}$) and Mo-$NHNH_2$. Step 2: Mo-$NHNH_2$ decomposes to active hydrogen species ($Mo^{\delta+}$-$H^{\delta-}$) and releases HN═NH via β-hydrogen elimination pathway. Step 3: the released HN═NH attacks another Mo ion and generates Mo–OH ($H^{\delta+}$) and Mo-N_2H. Step 4: Mo-N_2H releases N_2 and generates another active hydrogen species ($Mo^{\delta+}$-$H^{\delta-}$). Step 5: the $H^{\delta-}$ and $H^{\delta+}$ species react with the nitro group to generate an amine or with hydrazine to generate NH_3, restoring the catalytically active sites to the original state. Without nitrobenzene, the surface proton and hydride are unlikely to recombine to form hydrogen. Therefore, it is clear that MoO_2 has two key roles: (1) It abstracts hydrogen and stabilizes it on the surface, restricting active H* recombination. (2) It catalyzes the hydrogen transfer to nitrobenzene. Such ability of co-existing proton and hydride is usually attributed to precious metal catalysts, and seldom for metal oxides. The unique metallic function assured by the delocalized electrons may account for the excellent activity of MoO_2. As a result, MoO_2 shows exceptionally high chemoselectivity toward the nitro reduction over C═C, C≡C, and C≡N groups at room temperature and lower, down to 0 °C, rendering it as a promising catalyst for hydrogenation reactions.

4.2. Catalyst for $NaBH_4$ donor

Water as a green solvent to replace the conventional organic solvent presents many advantages in the organic synthesis. $NaBH_4$ is soluble in water and can be catalytically decomposed to reactive hydrogen species by catalyst such as metal including Cu and Ni, metal sulfide, reducible metal oxide and functional carbon materials, similar to the case of $N_2H_4{\cdot}H_2O$ [122–126]. Hupp et al. reported thin Co_9S_8 films on silicon and fluorine-doped tin oxide (FTO) for transfer hydrogenation of *m*-nitrophenol to *m*-aminophenol, which outperforms cobalt oxide as well as amorphous CoS_x [125]. Yu et al. synthesized 3D melamine sponge-Au/CeO_2 nanowire networks to realize in situ continuous reduction of 4-nitrophenol in a consecutive flow system with high activity and good stability [126]. However, the hydrogenation of nitroarenes in water using other metals such as Cu and Ni catalyst remains great challenging due to the formation of hydroxides (from reacting with water) and oxides (from oxidation by air) caused rapid deactivation [122,123]. Similar to the case in Section 3.4, Zhao et al. coated the surface of Ni/TiO_2 with hydrophobic carbon layer by a hydrothermal method to prevent the Ni active species from contacting with water [123]. As expected, the catalyst presents higher activity and improved stability in aqueous reaction system; and Ni hydroxide is not detected on the used and water-treated carbon-coated Ni/TiO_2. The carbon layer also protects metallic Ni from being oxidized when exposed to air.

Actually, functional carbon itself also can catalyses the hydrogenation of nitroarenes by $NaBH_4$. For example, Wang et al. reported S, N co-doped carbon nanotubes for transfer hydrogenation of *p*-nitrophenol by $NaBH_4$ [127]. As illustrated in Fig. 12a, the synthetic of carbon catalyst can be summarized as three steps: synthesis of CdS NWs as hard template; in situ self-polymerization of dopamine (PDA) on CdS surface; and carbonization of PDA and evaporation of Cd by annealing

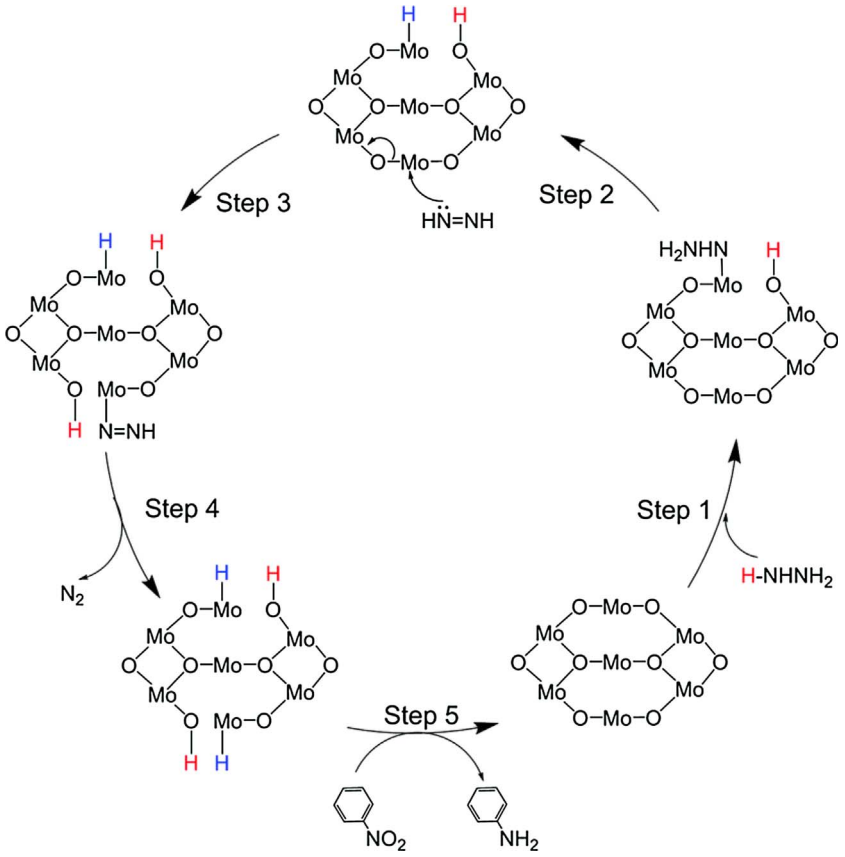

Fig. 11. Possible mechanism for catalytic N—H and N—N bond cleavage of hydrazine on MoO_2 surface in the nitrobenzene reduction. (reproduced from Ref. [119] with permission. Copyright 2016, Royal Society of Chemistry).

treatment at 1000 °C. With the presence of obtained catalyst (named as CP-1000), the reaction proceeds with a nearly 100% conversion and selectivity within 10 min at room temperature (20 °C), superior to S-doped and N-doped carbon and other reported metal-free catalysts (Fig. 12c). The apparent activation energy (E_a) is very low of 24.53 kJ mol^{-1} (Fig. 12b). DFT calculation shows carbon co-doped by S and N co-doped has the highest adsorption energy for *p*-nitrophenol (Fig. 12d), which accounts for the high activity.

As aforementioned, oxygen-deficient metal oxides can easily adsorb and activate nitroarenes, while metal nitride can decompose BH_4^- to produce reactive hydrogen species. Thus, nitrogen species and oxygen vacancies on the surface of metal oxide play synergetic roles in the transfer hydrogenation of nitroarenes. For example, Wang et al. reported TaO_xN_y hollow nanocrystals by nitridation of $Ta_{1.1}O_{1.05}$ that exhibit outstanding activity toward transfer hydrogen of nitrobenzenes [128]. In detail, the N species in catalyst surface can bind with BH_4^- to form metastable iminoborohydride (-N···*H*-BH_3) species, whereas oxygen vacancies act as the adsorption centers to capture the oxygen end of 4-nitrophenol. Then 4-nitrophenol is hydrogenated by coupling electron transfer and surface hydrogen species from -N···*H*-BH_3 to nitro group. Simultaneously, the BH_4^- ions help to release oxygen atoms from the lattice sites to regenerate the oxygen vacancies. This was verified by the recycling experiment, in which the reducing capacity of TaO_xN_y nanocrystals was well-reserved after five cycles of redox reactions.

4.3. Catalyst for HCOOH and alcohol donor

There are two subcategories: i.e., the monohydride and dihydride mechanisms for the catalytic decomposition of HCOOH and alcohol to produce reactive hydrogen species [107]. In the monohydride route, only the hydrogen on α-C of alcohols and HCOOH is transferred to metal catalyst. In contrast, the dihydride mechanism entails that both hydrogen atom in hydroxyl group and that bonded to α-C are transferred to the catalyst. The key difference between these two pathways is whether the hydrogen atoms in O—H and C—H maintain their identity in the product, which can be confirmed by isotopic tracer method.

Many metal-based catalysts such as Ni, Ni_3N and MoS_x can decompose HCOOH into CO_2 and H_2, thus nitroarenes may be reduced into corresponding anilines by in-situ formed active hydrogen species [129,130]. For example, Shalom et al. reported highly air stable sponge-like Ni-based catalysts (Ni and Ni_3N) embedded in a network of N-doped carbon by heating $NiCl_2$/LiCl/dicyandiamide molten salt system [129]. The carbon network with high surface area and homogenous pore distribution acts as not only an electronic activator but also a matrix to prevent the leaching of Ni and Ni_3N nanoparticles. Thus, such catalyst illustrates extraordinary activity and selectivity for transfer hydrogenation of nitrobenzene using HCOOH. Also, the Fe_2O_3- and Co_3O_4-based catalysts reported by Beller et al. can be used to activate HCOOH and give high selectivity for the reduction of nitro groups [131,132]. They also synthesized cubane-type Mo_3S_4 cluster ($[Mo_3S_4H_3(dmpe)_3]^+ \cdot Cl^-$, dmpe is 1,2-(bis)dimethylphosphinoethane) for the transfer hydrogenation of nitroarenes with HCOOH as donor [133], in which the molybdenum species are involved in the following catalytic cycle (Fig. 12e). Initially, Mo_3S_4 cluster chloride is used as the catalyst precursor, the chlorine atom is quickly replaced by formate to afford hydride active cluster via *β*-hydride elimination, accompanied by CO_2 release (step i and ii). Then, HCOOH reacts with the hydride site to generate unstable dihydrogen bonded species (step iii). Next, hydrogen is transferred from Mo centre to nitrobenzene to generate the formate-substituted cluster complex (step iv). As a result, reduction of a variety of nitroarenes to anilines can be achieved with > 99% conversions and 89–99% yields.

Alcohol also can function as hydrogen donor. For example, Keane et al. used Cu-SiO_2 as catalyst to couple 2-butanol dehydrogenation and nitrobenzene hydrogenation, showing 100% yield to both target

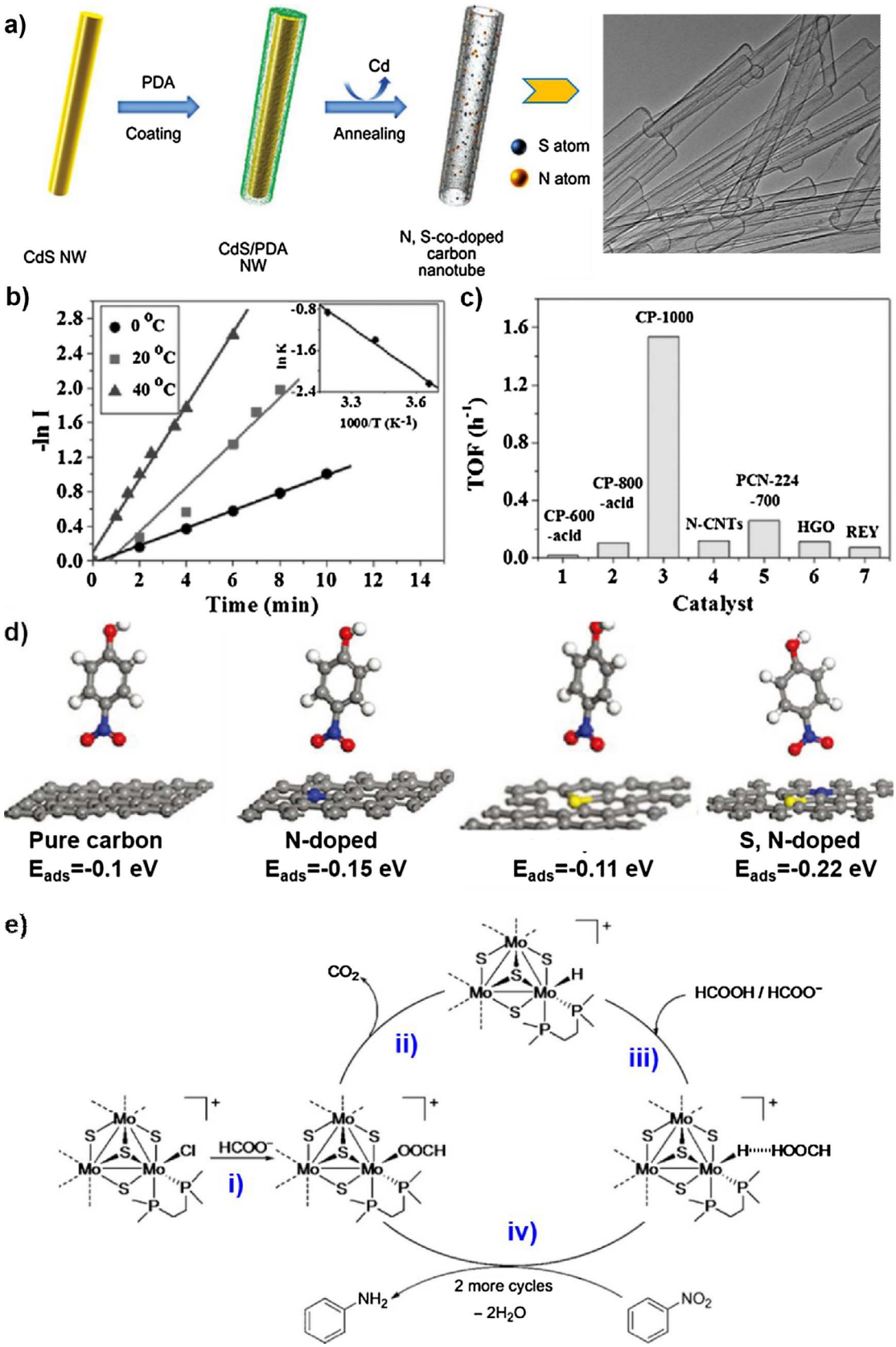

Fig. 12. (a) Synthesis process of S, N co-doped carbon nanotubes. (b) Arrhenius plots for reaction catalyzed by CP-1000. (c) Comparison of TOF for *p*-nitrophenol reduction with other metal-free catalysts. (d) Comparison of adsorption energies of nitrophenol on different carbon surfaces. (reproduced from Ref. [127] with permission. Copyright 2017, Wiley Online Library) (e) Proposed catalytic cycle for molybdenum cluster species involved in the reduction of nitrobenzene with formate/HCOOH as hydrogen donor. (reproduced from Ref. [133] with permission. Copyright 2012, Wiley Online Library).

products (2-butanone and aniline) with appreciably (by a factor of 50) enhanced hydrogen utilization as comparable to conventional nitrobenzene reduction using pressurized H_2 [134]. The result indicates the generation of reactive hydrogen associated with the metal sites (Cu-H) is effectively transferred for $-NO_2$ reduction compared with the limitations associated with H_2 activation/dissociation. Li et al. reported a MOF-derived Co/N−C hybrid for transfer hydrogenation of nitroarenes using isopropanol as donor [135]. Experimental results confirm the importance of both metal (Co) and basic sites of N species from triethylenediamine ligand for achieving high catalytic efficiency in transfer hydrogenation. In contrast, Co-C material is not active in this transformation due to the lack of basic sites on the carbon support.

5. Photocatalyst for hydrogenation of nitroarenes under light

5.1. Fundamentals of photocatalytic hydrogenation of nitroarenes

In addition to thermal catalytic hydrogenation routes, photocatalytic and electrocatalytic hydrogenation have attracted increasing attentions, which can be driven by solar energy, or solar-, wind- and other renewable resources-derived electricity. In fact, solar and wind technologies are booming worldwide, especially in China, Europe, the United States and Japan [136]. Photocatalyst is the key to produce hydrogen species from the hydrogen donors that is also called hole scavenger including alcohol, ammonium formate, oxalic acid, ammonium oxalate, and triethanolamine, and so on [137]. Upon illumination, photocatalyst produces photoinduced electrons and holes, then migrating to the surface. Next, the holes oxidize the alcohol, as an example, to produce ketone and protons, and meanwhile the reduction of nitroarene by proton-coupled electrons produces the corresponding anilines. Note that, in addition to the common factors such as the formation of hydrogen species and activation of nitro group in other hydrogenation routes, charge separation and combination is another determining factor for the overall hydrogenation activity. According to the difference of light absorber, three kinds of photocatalytic systems such as semiconductor, plasmonic and dye-sensitized photocatalyst can be included.

5.2. Semiconductor photocatalyst

TiO_2 is the most widely studies photocatalyst, including the photocatalytic hydrogenation of nitroarenes with alcohol as hydrogen donor under inert gas atmosphere [138–140]. Photocatalytic hydrogenation of nitroarenes by TiO_2 was first studied by Li et al. [141]. The reduction of 6-nitrocoumarin gave 6-aminocoumarin in 79% yield under the irradiation of a suspension of TiO_2 in ethanol. This simple method is applicable to the reduction of a wide variety of nitroarenes. Zhang et al. further reported N-doped TiO_2 catalyst for photocatalytic hydrogenation of nitroarenes with methanol as hydrogen donor [142]. Note that early reported systems use TiO_2 such as anatase or P25 as photocatalyst, having insufficient activity and selectivity due to the poor charge separation and quite weak adsorption strength of nitroarenes [141,143,144]. The introduction of oxygen vacancy within TiO_2 can promote charge separation and adsorption of nitroarenes. Shiraishi et al. thus reported oxygen vacancies on rutile surface can promote the adsorption of nitroarene on Ti^{3+} atoms and enhance the trap of photoinduced electrons, enabling aniline formation with significantly high quantum yield [140]. Also, selective reduction of nitroarene to functionalized anilines with > 94% yield can be obtained. It is well-known that TiO_2 has two common polymorphic forms: anatase and rutile [145,146]. Anatase usually exhibits higher photocatalytic activity than rutile, and its activity is further improved by coupling with about 20% rutile, which is available as commercial P25 by Degussa synthesized by hydrogen flame combustion of $TiCl_4$ [147,148]. However, both anatase and P25, show lower activity and selectivity than rutile TiO_2 for the reduction of nitroarene [140]. Shiraishi et al. further reported that rutile particles isolated from P25 by HF treatment shows higher hydrogenation activity than commercially available rutile TiO_2 [139]. The isolated rutile particles contain a relatively small number of inner defects behaving as charge recombination centers, and a relatively large number of surface defects behaving as active sites for nitro adsorption.

Also, to overcome the drawback of wide-bandgap TiO_2 utilizing only UV light, other visible-response narrow-bandgap semiconductors such as CdS have been reported for photocatalytic hydrogenation of nitroarenes with excellent activity [137]. For example, Xu and Xiao et al. reported graphene/CdS composites for selective reduction of nitroarene with different substituent groups under visible light irradiation [149,150]. The composite exhibits higher activity than bare CdS, mainly because graphene significantly enhances the adsorption of substrates and promotes the charge carrier separation that thus increases the probability of photoinduced electrons participating in the photocatalytic hydrogenation. In addition, the photocorrosion of CdS is efficiently inhibited by controlling the reaction conditions, i.e., using ammonium formate ($HCOONH_4$) as hole scavenger and N_2 atmosphere.

5.3. Plasmonic photocatalyst

TiO_2 photocatalyst has a high oxidation potential (2.7 V) and maybe exhibit poor selectivity due to the excessive additional photooxidiation. Actually, it is difficult to adjust the oxidation potential of semiconductor in order to tune the selectivity. In addition, it only utilizes UV light due to the wide bandgap (3.2 eV). In contrast, plasmonic metal NPs like Au, Ag and Cu can strongly absorb visible light because of the localized surface plasmon resonance (LSPR) effect [151]. This effect is the collective oscillation of conduction electrons, which resonate with the electromagnetic field of incident light and result in significant enhancement of the local electromagnetic fields near rough surfaces of metal NPs. When coupled with semiconductor, the interfacial electrons are transferred from plasmonic metal to the conduction band of metal oxide for the proton/electron coupled reduction of nitroarenes. Meanwhile, the LSPR excitation induces modest oxidation ability on the plasmonic metal surface [24,152]. To date, the moderate catalyzing properties and visible light absorption of plasmonic metal have been widely reported to facilitate photocatalytic hydrogenation [153–158]. Also, plasmonic materials have been extended to nonmetallic nanocrystals like Cu-deficient $Cu_{2-x}S$, $Cu_{2-x}Se$ and Sb-doped SnO_2 [159].

The most representative “plasmonic photocatalyst” for the hydrogenation of nitroarenes is Au/TiO_2. For example, Tada et al. reported TiO_2-supported Au NPs with a bimodal size distribution (BM-Au/TiO_2) for the photocatalytic one-step synthesis of azobenzenes from nitrobenzenes (Fig. 13) [153]. Note it is an amazing finding, because in thermalcatalysis, two-step reaction are necessary to proceed with high-pressure H_2 and O_2 respective responsible for hydrogenation of nitrobenzene to aniline and oxidative coupling of aniline to azobenzene [24]. In detail, large Au NPs (with mean large particle size of about 9 nm) are loaded on rutile TiO_2 (L-Au/TiO_2) by deposition-precipitation method. Then $[Au(OH)_3Cl]^-$ complex ions are adsorbed on TiO_2 surface of L-Au/TiO_2 and reduced by $NaBH_4$ to yield small Au NPs (with mean small particle size of about 2 nm). From UV–vis absorption spectra (Fig. 13d), Au/TiO_2 shows broad LSPR-absorption around 550 nm, well resembling the solar light spectrum. For the photocatalytic hydrogenation, TiO_2 loaded with either small Au particles (S-Au/TiO_2) or large Au particles (L-Au/TiO_2) is inactive (Fig. 13a). Surprisingly, BM-Au/TiO_2 exhibits a high visible-light activity, with the yield of azobenzene reaching 95% and acetone generated as a result of 2-propanol oxidation (Fig. 13b). Azoxybenzene is generated with azoxybenzene as an intermediate, while the amount of aniline is negligibly small. Based on photodeposition experimental, the LSPR excitation of BM-Au/TiO_2 causes the net electron transport from S- to L-Au NPs through the conduction band of TiO_2 (Fig. 13e). The intimate contact between Au NPs and TiO_2 with a large contact area favors the interfacial electron transfer. As a result of the long-distance charge

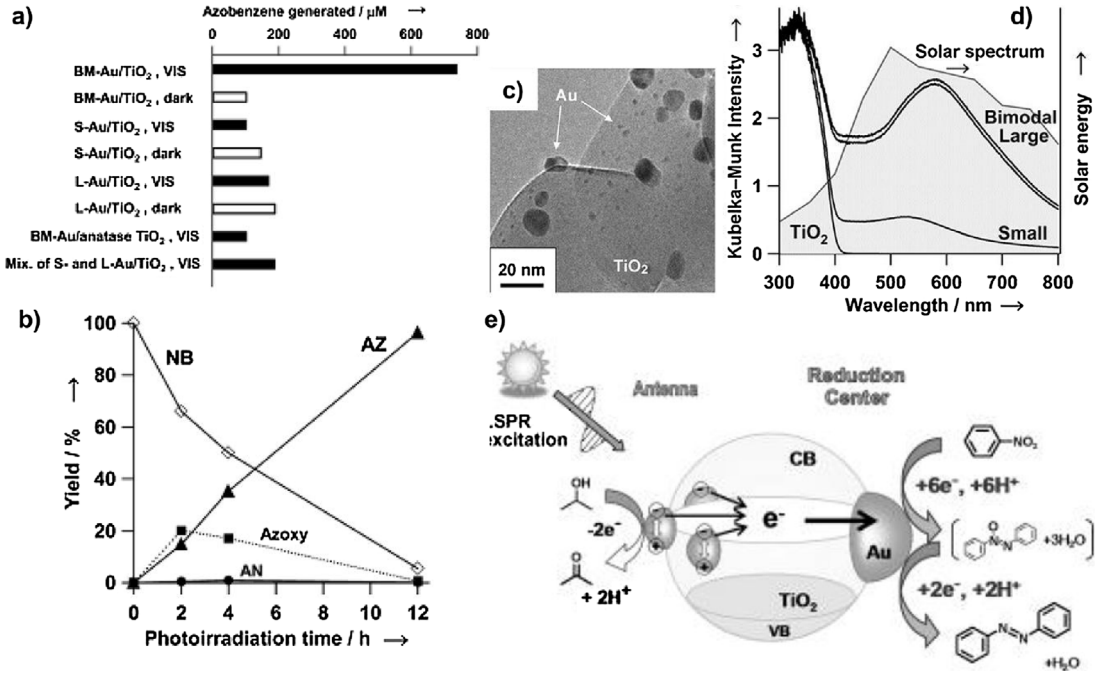

Fig. 13. (a) Azobenzene formed at 2 h reaction time by using various Au/TiO_2. (b) Time-dependent for nitrobenzene reduction by BM-Au/TiO_2. (Reaction conditions: BM-Au/TiO_2 10 mg, nitrobenzene (10 mM) solution (10 mL, 2-propanol) with KOH (10 mM), visible-light ($\lambda > 430$ nm, 10 mW cm^{-2}) irradiation at 25 °C under aerobic conditions.) (c, d) TEM image and UV–vis absorption spectra of BM-Au/TiO_2, respectively. (e) Mechanism for the photocatalytic hydrogenation of nitroarene. (reproduced from Ref. [153] with permission. Copyright 2014, Wiley Online Library).

separation over about 40 nm, the surfaces of S- and L-Au NPs efficiently work as the oxidation and reduction sites, respectively. Nitrobenzene is strongly adsorbed through the nitro group at the interface between the Au NP and TiO_2. In those sites around L-Au NPs, nitrobenzene undergoes eight-electron and proton-coupled reduction to azobenzene via azoxybenzene by electron pool effect. On the other hand, isopropanol is oxidized to acetone on the surface of S-Au NPs.

Zhu et al. reported 3 wt% Au/ZrO_2 (Au nanoparticles with size of 6 nm) for photocatalytic hydrogenation of nitroarene under visible light (Fig. 14) [154]. Interestingly, it is found that oxygen is released as an unforeseen by-product, indicating that the photocatalytic hydrogenation proceeds by a mechanism different from that of BM-Au/TiO_2, because the LSPR excitation-induced interfical electron transfer from Au NP to the high conduction band of ZrO_2 cannot occur [160]. Based on time-dependent product distribution (Fig. 14b), this reaction involves two processes: first isopropanol is oxidized to acetone; then nitrobenzene is reduced to azobenzene with azoxybenzene as intermediate. After the initial reaction stage, the oxidation of isopropanol should cease when the surface of AuNPs becomes saturated with H-AuNP and HO-AuNP species, and the content of acetone remains unchanged (see overall reaction in Fig. 14). The oscillating electrons interact strongly with the electrophilic nitro groups of nitrobenzene, and assist the cleavage of N—O bonds by H-AuNP species on AuNPs. The HO-AuNP species can release oxygen gas and transform into H-AuNP species that can be recycled in the subsequent reaction.

Copper can also gain visible light energy through the LSPR effect, however, the primary challenge for Cu nanoparticles to be used as photocatalyst is their chemical instability under reaction conditions. Graphene is a two-dimensional network of sp^2-bonded carbon atoms; and the delocalized electrons in graphene can move freely in the network with a low resistance. The carbon vacancies or dangling bonds in graphene can influence the electronic structure of Cu atoms and improve their chemical stability. Based on these, Guo et al. synthesized Cu/graphene by reducing Cu_2O/graphene for the reduction of nitroarenes under visible light [158]. The hydrogenation produces azobenzene with a yield of 96% at 90 °C. When illuminated with natural sunlight (mean light intensity of 44 mW cm^{-2}) at 35 °C, 70% of nitrobenzene is converted and 57% of the product is azobenzene. Due to the production of O_2, the mechanism is very similar to that proposed by Zhu et al. [154].

According to the energy distribution in the solar spectrum, around 54.3%, 38.9%, and 6.8% of sunlight at the earth's surface is located in the near infrared (NIR, 760–3000 nm), visible (vis, 400–760 nm), and ultraviolet (UV, < 400 nm) range, respectively. Therefore, the development of photocatalyst with NIR absorption, low cost, high stability, and outstanding catalytic performance is highly desirable for solar photosynthesis. Copper chalcogenide nanocrystals with excellent plasmonic absorption especially in the NIR region are promising candidates for building plasmonic photocatalysts [159]. For example, Huang et al. reported the synthesis of composite photocatalyst containing both noble metal (Pd) and Cu_7S_4 domains with intimate interfacial contact [161]. These Cu_7S_4@Pd nanocrystals, by combining NIR LSPR light-harvesting property of Cu_7S_4 with the catalytic features of Pd, are excellent catalysts for photocatalytic hydrogenation of nitrobenzene. In detail, the strong NIR plasmonic absorption of Cu_7S_4@Pd facilitates hot holes transfer from Cu_7S_4 to Pd due to the formation of Schottky barrier, which subsequently promote the catalytic reaction on Pd surface. In the hydrogenation reaction, Pd is generally considered active catalyst but suffers from rapid surface-poisoning due to strong binding of H atoms. Previous studies suggested negative charges can enhance the binding of H atoms on Pd surface, while positive charges help with dissociation of adsorbed H atoms. Hence, the transferred hot holes can facilitate hydrogenation reaction through promoting H atom dissociation and thus keep Pd surface consistently active, leading to enhanced catalyst activity with good stability.

5.4. Dye sensitized photocatalyst

Organic dye can absorb visible light to generate an excited state (dye*), which injects an electron into the conduction band of semiconductor and ultimately transfers it to an electron acceptor (for example: nitroarenes) through the conduction band. Meanwhile, the

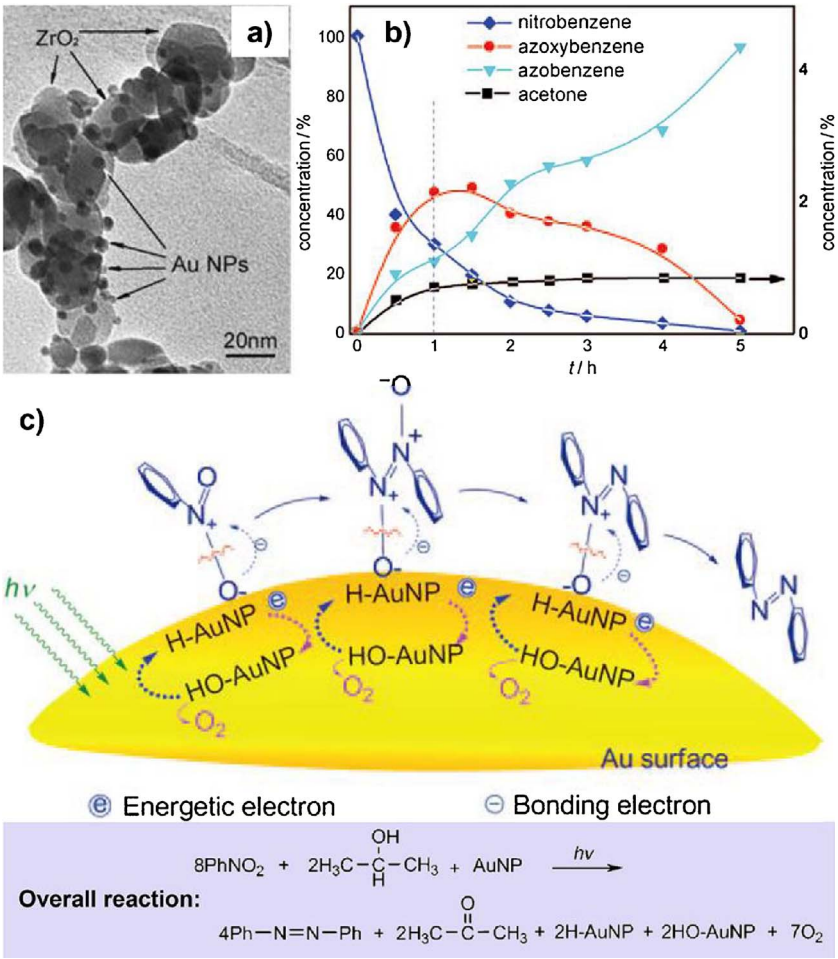

Fig. 14. (a) TEM images and (b) Photocatalytic activity of 3 wt% Au/ZrO_2. (Reduction reaction was conducted in an argon atmosphere at 40 °C using 30 mL of isopropanol mixed with 0.3 mmol KOH, 3 mmol nitrobenzene, and 100 mg catalyst.) (c) Mechanism for photocatalytic hydrogenation of nitroarene. (a–c reproduced from Ref. [154] with permission. Copyright 2010, Wiley Online Library).

positive charge is left on the dye molecule to produce Dye^+ free radical, which can be regenerated by other scavengers such as triethanolamine [162,163]. For example, a visible light absorbing surface complex can be formed when the colourless organic molecule, 2,3-dihydroxynaphthalene (2,3-DN) is adsorbed on the surface of anatase TiO_2 via the strong bonding of the *ortho* dihydroxyl on the aromatic ring. When used in combination with a common reduction co-catalyst Pt NPs, the surface complex could photocatalyze the reduction of nitrobenzene to aniline with triethanolamine (TEOA) when exposed to $\lambda > 420$ nm visible light irradiation from a 500 W Xe lamp (Eq. (1)) [164]. An organic dye **N3** in combination with TiO_2 (Degussa P25) along with the assistance of Pt NPs, produced in situ from K_2PtCl_6, can also effectively reduce nitrobenzene into aniline with TEOA when exposed to the visible light irradiation from 530 nm LEDs (Eq. (2)) [165]. Interestingly, without the presence of K_2PtCl_6 as the reducing cocatalyst, the reaction rate for the reduction of nitrobenzene to aniline could be augmented by adding trace amount of urea derivatives as the cocatalyst, which is ascribed to the provision of additional proton shuttling channels by urea derivatives [166].

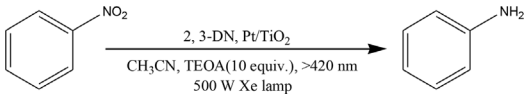

(1)

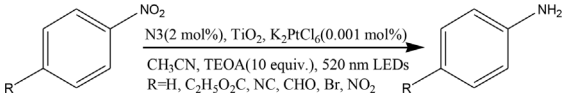

(2)

Some organometallic complexes of ruthenium(II) and iridium(III), and purely organic dyes have also been directly adopted in visible-light induced organic transformations without the assist of metal oxide semiconductor [167–170]. For example, Zheng and Wu et al., recently, reported a simple but efficient photocatalytic nitrobenzene reduction employing Eosin Y as photocatalyst and TEOA as hole scavenger [171]. With green LED light irradiation, the nitro groups in nitrobenzenes are selectively reduced in quantitative yields. The photoinduced electron transfer mechanism suggests that the high selectivity originates from the better electron-withdrawing ability of the nitro group.

6. Catalyst for electrocatalytic hydrogenation of nitroarene

6.1. Fundamentals of electrocatalytic hydrogenation of nitroarene

Similar to elelctrocatalytic reduction of CO_2 [172], the reduction of nitroarene in aqueous solution can be operated in a three-electrode and two-home cell, in which the cathodic reaction brings about the reduction of nitroarene to aniline, while the anodic reaction is associated with water oxidation (Fig. 15a) [173]. That is, the proton from water oxidation ($2H_2O \rightarrow 4H^+ + O_2$) coupled with electron drive the overall hydrogenation process. Typically, the operated potential range is at the scope of hydrogen evolution from water splitting (0 V vs. RHE). Thus, the reduction of nitroarene and water are two competitive reactions. The common notions in electrocatalytic hydrogenation of nitroarene include peak potential, peak current and faradaic efficiency, similar other electrocatalytic processes [172].

6.2. Electrocatalyst for hydrogenation of nitroarene

The key to obtain highly-efficient electrocatalytic hydrogenation of nitroarene is seeking and fabricating suitable cathodic materials. Up to

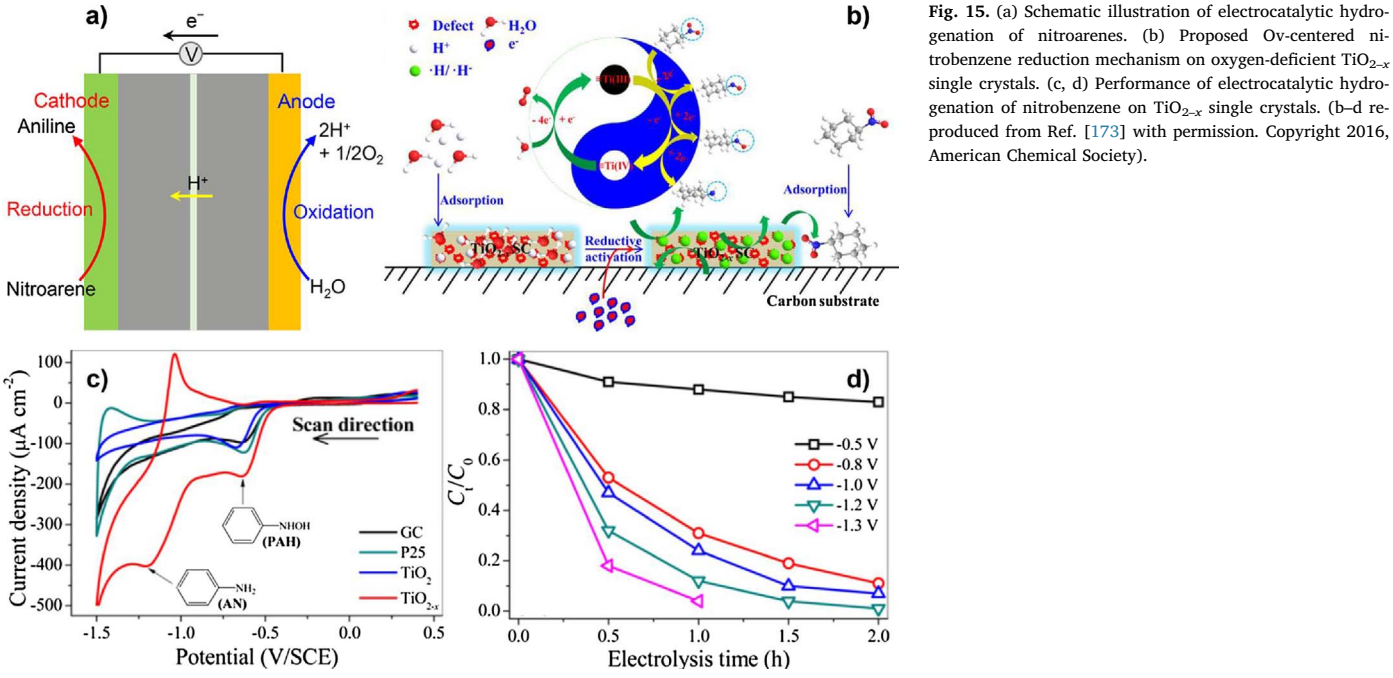

Fig. 15. (a) Schematic illustration of electrocatalytic hydrogenation of nitroarenes. (b) Proposed Ov-centered nitrobenzene reduction mechanism on oxygen-deficient TiO_{2-x} single crystals. (c, d) Performance of electrocatalytic hydrogenation of nitrobenzene on TiO_{2-x} single crystals. (b–d reproduced from Ref. [173] with permission. Copyright 2016, American Chemical Society).

now, various metallic cathodic materials have been developed for this purpose, for example, nobel-metal of Pd, Pt, and Ag and non-noble metals of Fe, Cu, and Ni [174,175]. Jiang et al. reported Cu-based catalyst for electrocatalytic hydrogenation of nitrobenzene [176]. They choose $Cu_{70}Zr_{30}$ alloy as precursor and activated it by selective dissolution of Zr atoms using chemical etching. The obtained amorphous alloy is effective electrocatalyst for the reduction of nitrobenzene to aniline due to the formation of Cu-rich surface and enlarged electrochemical active surface area compared with pristine $Cu_{70}Zr_{30}$ alloy.

The products (including aniline, nitrosobenzene, phenylhydroxylamine, azoxybenzene, hydrazobenzene, benzidine, *p*-aminophenol and quinone) are sensitive to reaction conditions and so the control of the electrolysis to obtain a single product remains a challenge [177,178]. In acidic media the electroreduction of nitrobenzene on solid cathodes (Cu, Pb and Hg) gives *p*-aminophenol in yield ranging from 15 to 81% besides aniline and azoxybenzene [179,180]. Under alkaline and neutral conditions, aniline has been observed to form at various electrodes along with azoxybenzene, azobenzene and hydrazobenzene via the condensation hydrogenation route [181,182].

In addition to metal, some cheap and stable metal oxides such as TiO_2 have been reported for the electrocatalytic hydrogenation of nitroarene [173,183]. Recently, Yu et al. reported oxygen-deficient TiO_{2-x} single crystals dominantly exposed by high-energy [001] facet facets as cathode for electrocatalytic hydrogenation of nitrobenzene (Fig. 15b) [173]. From cyclic voltammogram (CV) curves, the reductive current of 10 mg L^{-1} nitrobenzene aqueous solution with 0.1 M Na_2SO_4 (no pH adjustment) on black electrode (GC), P25 and TiO_2 electrode are very low, and only a reduction peak ($4e^-$ reduction peak from $PhNO_2$ to PhNOH) is observed at ca. −0.60 V (vs. SCE). In comparison, the reductive current is significantly increased and an additional reduction peak ($2e^-$ reduction peak from PhNOH to $PhNH_2$) appears at ca. −1.15 V on the TiO_{2-x} electrode (Fig. 15c). Furthermore, the time-dependent electrolysis at different bias on TiO_{2-x} electrode confirms this voltammogram (Fig. 15d), and nitrobenzene concentration is substantially decreased when the applied bias is negative than −0.6 V, while it is less than 20% with the bias of −0.5 V. This result might be attributed mainly to electroassisted adsorption, a nonfaradic process irrelative to any electron transfer. Also, the cathodic potential of −1.3 V is negative than the potential of molecular hydrogen evolving observed in electrolysis period, substantially lowering the current efficiency. In this process, the surface-adsorbed atomic H* is the main active species for the nitrobenzene reduction at the TiO_{2-x}/C electrode, and the atomic H*-mediated indirect pathway plays a dominant role and only a minor nitrobenzene reduction is achieved by the direct electron transfer mechanism (Fig. 15b). Furthermore, the reductive regeneration of reactive ≡Ti(III) from oxidized ≡Ti(IV) on the carbon cathode may be the rate-limiting step for electrocatalytic hydrogenation. Notably, due to the improved electric conductivity, decreased charge transfer resistance and versatile redox crystal structure to accommodate both reduced ≡Ti(III) and oxidized ≡Ti(IV) in oxygen-deficient TiO_{2-x}, the in situ regeneration of reactive ≡Ti(III) centers should be favored without any substantial structural constrain for continuous cathodic reaction. Also, the electroassisted adsorption of organic pollutants onto carbon substrate could facilitate the electrochemical hydrogenation in the vicinity of H-saturated TiO_{2-x}.

Functional carbon materials also can be used as electrocatalyst for the reduction of nitroarene [184,185]. For example, Guo et al. reported the synthesis of multi-wall carbon nanotubes (MWNTs) modified glassy carbon electrodes (MWNTs/GCEs) and investigated the influence of surface modifications to the reduction of nitrobenzenne in acid electrolytes [185]. The MWNT samples were modified included pristine MWNT (MWNT-P), acid-treated MWNT (MWNT-T, containing carboxylic groups with a small part of hydroxyl groups) and hydroxyl-containing MWNT (MWNT-OH). Experimental results showed that hydroxyl-containing MWNTs exhibited the highest electrocatalytic activity among the used MWNTs because of its weak capacitive features and oxygen-containing functional groups.

7. Conclusions and perspectives

Catalytic hydrogenation of nitroarenes is very important for dyestuffs and pharmaceuticals in chemical industry. In the past decade, great breakthroughs have been made on the design and synthesis of nanostructured materials towards the catalytic selective hydrogenation of nitroarenes, including metal, metal oxide, sulfide/carbides, nitrides and boride, and functional carbon material. Also, based on the difference of hydrogen source, catalytic hydrogenation of nitroarenes can be classified as: direct catalytic hydrogenation using high-pressure hydrogen (Table 1); catalytic transfer hydrogenation using reductive compounds such as hydrazine, $NaBH_4$, alcohols and formic acid

Table 1
Catalytic performances for direct hydrogenation of nitroarene catalyzed by some representive catalysts.

Catalyst	Reactant	*T* (°C)	*P* (bar)	Time (h)	Conversion (%)	Selectivity (-NH_2, Azo,[a] -NHOH,[b] %)	Ref.
Au/TiO_2	3-nitrostyrene	120	9	6	98.5	95.9	[5]
	4-nitrobenzaldehyde	100	10	1.25	99	96.8	
	4-nitrobenzonitrile	140	25	1.25	99	97.2	
	4-nitrobenzamide	120	15	3	99.6	97.3	
	1-nitro-1-cyclohexene	110	15	0.5	99.6	90.9	
Ni/AC_{OX}	3-nitrostyrene	40	3	3.17	97.9	97.1	[41]
	4-nitrobenzaldehyde			2.67	100	90	
$Ni@PS_{60}SiCN$	4-nitrobenzaldehyde	110	50	20	99	99	[49]
	3-nitrobenzonitrile						
Co-SiCN	4-nitrobenzaldehyde	110	50	15	99	99	[50]
Pt/FeO_x	3-nitrostyrene	40	3	0.83	96.5	98.6	[40]
	4-nitrobenzaldehyde			0.5	99.5	92.8	
	4-nitrobenzonitrile			2	90.3	97.8	
Co−N−C	nitrobenzene	80	30	1.5	100	97[a]	[52]
PdsNC/*PN*-CeO_2	4-nitrophenol	80	5	2	100	100	[48]
Pt-PMA/AC	nitrobenzene	100	10	1	33.3	100	[56]
1.5%Au@0.01%Pt/TiO_2	3-nitrostyrene	85	8	0.52	94.5	93.4	[26]
EDA-Pt NW	nitrobenzene	25	0.5	0.83	100	100[b]	[25]
$WO_{2.72}$	4-nitrobenzaldehyde	150	30	15	91.6	100	[32]
Fe_2O_3	3-nitrostyrene	120	50	16	96	93	[9]
	4-nitrobenzonitrile	105		26	75	100	
NiPB	4-nitrochlorobenzene	80	12	0.67	97	100	[92]
$CN/Ni/Al_2O_3$	3-nitrobenzenesulfonic	120	10	2	100	100	[95]
CoO_x@NCNTs	3(4)-nitrobenzonitrile	110	30	3	99	99	[100]
	3-nitrostyrene						
	4-nitrochlorobenzene						

(Table 2); photocatalytic hydrogenation using hole scavenger (Table 3); electrocatalytic hydrogenation accompanied with water oxidation. For these technologies, most of the reported catalysts can selectively hydrogenate nitroarenes into anilines with the maintaining substituted groups. Interestingly, some plasmonic photocatalysts such as BM-Au/TiO_2, Au/ZrO_2 and Cu/graphene can one-step selectively hydrogenate nitroarenes into azobenzenes, an important organic dyes, indicators, food additives, and therapeutic agents. More intriguingly, thylenediamine (EDA)-coated ultrathin Pt nanowires (EDA-Pt NWs) can readily induce a perfect interfacial electronic effect to shape their catalytic selectivity for the production of phenylhydroxylamine, a thermodynamically unfavorable but industrially important compound.

For the direct hydrogenation using H_2, the production of reactive hydrogen species and preferential adsorption of nitro group of nitroarenes on catalyst surface can be achieved by finely tuning the structure in nanoscale, including: (1) Metal-support interaction, size effect, single-atom, alloy effect, shape-selective catalysis, strain effect and interfacial adsorbent-metal interaction for metal; (2) Defect engineering and metal oxide/N-doped carbon interaction for metal oxide; (3) Interfacial electronic effect for carbon material. Most state-of-the-art noble-metals and bimetals exhibit excellent activity, but their commercial application is limited by their high costs, low abundance and poor selectivity. While non-noble metals and bimetals, for example, Co, Cu, and Ni, have a relatively low activity and poor stability. Metal oxides and functional carbon materials exhibit excellent selectivity, but their performance is still unsatisfied, and quite high-pressure hydrogen and high reaction temperature are still required. Although catalytic transfer hydrogenation and photocatalytic and electrocatalytic

Table 2
Catalytic performances for the transfer hydrogenation of nitroarene catalyzed by some representive catalysts.

Catalyst	Reactant	Donor	Atmosphere	T (°C)	Time (h)	Conversion (%)	Selectivity (-NH_2, %)	Ref.
$Co\text{-}Mo_2C$	4-nitrochlorobenzene	$N_2H_4{\cdot}H_2O$	air	25	2	100	100	[109]
	3-nitrobenzaldehyde					100	100	
Fe_3O_4	4-nitrochlorobenzene	$N_2H_4{\cdot}H_2O$		150	2 (min)	100	98	[110]
CeO_2	nitrobenzene	$N_2H_4{\cdot}H_2O$	air	80	3	100	76	[114]
	3-nitrobenzaldehyde					100	100	
O-doped carbon	4-nitrobenzophenone	$N_2H_4{\cdot}H_2O$	Ar	130	24	99	79	[115]
	4-nitrochlorobenzene					99	72	
RGO	nitrobenzene	$N_2H_4{\cdot}H_2O$		80	4	100	94.2	[108]
MoO_2	nitrobenzene + styrene	$N_2H_4{\cdot}H_2O$	air	0	0.5	99	99	[119]
Co_9S_8	3-nitrophenol	$NaBH_4$	air	25	15 (min)	99	100	[120]
S,N co-doped CNs	4-nitrophenol	$NaBH_4$	air	20	10 (min)	100	100	[127]
TaO_xN_y	4-nitrophenol	$NaBH_4$	air	25	45 (min)	91.3	100	[128]
	3-nitrobenzaldehyde				30 (min)	70	100	
Ni/Ni_3N	nitrobenzene	HCOOH	air	85	2	99	100	[129]
Fe_2O_3/NGr	3-iodonitrobenzene	HCOOH		120	12	99	94	[131]
Co_3O_4/NGr	nitrobenzene	HCOOH		100	15	100	96	[132]
Mo_3S_4	nitrobenzene	HCOOH		70	10	99	99	[133]
	3-nitrobenzaldehyde				18	99	90	
	4-nitrobenzophenone				18	99	99	
Cu/SiO_2	nitrobenzene	2-butanone	N_2	200		100	100	[134]
Co/N−C	nitrobenzene	isopropanol		150	50	80	99	[135]
	4-nitrochlorobenzene				60	95	99	

Table 3
Catalytic performances for photocatalytic hydrogenation of nitroarene catalyzed by some representive catalysts.

Catalyst	Reactant	Donor	Atmosphere	T (°C)	Time (h)	Conversion (%)	Selectivity (-NH_2, Azo,[a] %)	Photonic efficiency (%)	Ref.
Rutile TiO_2	nitrobenzene	isopropanol	N_2	30	3	97	94		[139]
	4-nitrochlorobenzene				4	99	96		
	3-nitrobenzaldehyde				5	99	94		
	3-nitrostyrene				6	99	94		
Ag/TiO_2	nitrobenzene	CH_3OH		25	1	84.3	100		[152]
Au/TiO_2[a]	nitrobenzene	isopropanol	Ar	40	12	95	99		[153]
Au/ZrO_2[a]	nitrobenzene	isopropanol	Ar	40	5	100	99	6.9	[154]
Cu/graphene[a]	nitrobenzene	isopropanol		90	5	97.9	98.2	5.1	[158]
Cu_7S_4@Pd	nitrobenzene	H_2	1 bar	30 ~ 60	0.5	100			[161]
Eosin Y	nitrobenzene	TEOA	Ar	25	24	99	99		[171]
	4-nitrochlorobenzene					99	98		
	4-nitrobenzaldehyde					100	100		
	2(3, 4)-nitrobenzonitrile					99	100		

a represents as the product of azobenzene.

hydrogenation open a door for the hydrogenation of nitroarenes under mild condition such as room temperature and atmosphere, but the separation of target product from the hydrogen donor and hole scavenger is more difficult. Electrocatalytic hydrogenation requires high overpotential and is competitive with hydrogen evolution. Therefore, more researches are still needed which can be directed along the following aspects:

1) **Identification of active sites of catalyst.** There are generally two strategies to improve the activity of a catalyst: (i) increasing the number of active sites on a given catalyst (e.g., through nanostructuring to expose more active sites) or (ii) increasing the intrinsic activity of each active site. Thus, identification of the nature of the active site is important and should be the first step in the design of an efficient catalyst. For example, Beller et al. reported the Fe-, Co- and Ni-based oxides for the selective hydrogenation of nitroarenes with excellent activity and stability, but the real active site is underway and absence of direct evidences [7,9,83]. For this reason, the development of in situ characterization techniques is crucial, since they can possibly disclose more key information regarding the intermediate and active sites, therefore provide guidance for subsequent catalyst design. Some techniques such as scanning probe microscopy, ambient pressure X-ray photoelectron spectroscopy and soft X-ray absorption spectroscopy may have the potential to realize the purpose of in situ characterization.
2) **Better understanding the mystery of catalytic selectivity.** To date, many reported catalysts can be used for selective hydrogenation of nitrobenzene to aniline in terms of intermediate products such as nitrosobenzene, phenylhydroxylamine and azo(xy)benzenes. Actually, the meaning of selectivity also includes the avoidance of reducible groups such as −C═C, −CHO substituted in nitroarenes being hydrogenated, especially in photocatalytic and electrocatalytic processes. In regard to this, more theoretical framework such as adsorption energy and reaction barrier and surface techniques such as in-situ attenuated total reflection infrared spectra (ATR-IR) should be performed to demonstrate the adsorption of substrate and the step-by-step hydrogenation.
3) **Extension from academic studies to industrial production.** So far academic studies mainly focus on the performance, selectivity and stability for the hydrogenation of nitroarenes at the catalytic material level. Consideration for industrial production of such catalytic materials is rare. Note that most of the powder catalysts with extremely high performance are nanostructured catalysts, which have a high cost due to the expensive precursors and complicated process. In addition, many such processes can only produce small quantities of product. Moreover, the sustainable separation and reuse of nanostructured catalysts remain a challenge [186]. Soon, a scalable process suitable for large scale production of low-cost, efficient and easy-separated catalytic material is needed.

Acknowledgements

The authors appreciate the supports from the National Natural Science Foundation of China (U1462119, U1463205), and the Tianjin Municipal Natural Science Foundation (16JCQNJC05200).

References

[1] A.-M. Alexander, J.S. Hargreaves, Chem. Soc. Rev. 39 (2010) 4388–4401.
[2] A. Corma, P. Concepcion, P. Serna, Angew. Chem. Int. Ed. 46 (2007) 7266–7269.
[3] M. Boronat, P. Concepcion, A. Corma, S. Gonzalez, F. Illas, P. Serna, J. Am. Chem. Soc. 129 (2007) 16230–16237.
[4] A. Corma, P. Serna, P. Concepcion, J.J. Calvino, J. Am. Chem. Soc. 130 (2008) 8748–8753.
[5] A. Corma, P. Serna, Science 313 (2006) 332–334.
[6] A. Burawoy, J. Critchley, Tetrahedron 5 (1959) 340–351.
[7] F.A. Westerhaus, R.V. Jagadeesh, G. Wienhofer, M.M. Pohl, J. Radnik, A.E. Surkus, J. Rabeah, K. Junge, H. Junge, M. Nielsen, A. Bruckner, M. Beller, Nat. Chem. 5 (2013) 537–543.
[8] A. Corma, P. Serna, Nat. Protoc. 1 (2006) 2590–2595.
[9] R.V. Jagadeesh, A.E. Surkus, H. Junge, M.M. Pohl, J. Radnik, J. Rabeah, H. Huan, V. Schunemann, A. Bruckner, M. Beller, Science 342 (2013) 1073–1076.
[10] B. Hammer, J.K. Nørskov, Adv. Catal. 45 (2000) 71–129.
[11] A. Vojvodic, J.K. Nørskov, Natl. Sci. Rev. 2 (2015) 140–149.
[12] K. Honkala, A. Hellman, I.N. Remediakis, A. Logadottir, A. Carlsson, S. Dahl, C.H. Christensen, J.K. Nørskov, Science 307 (2005) 555–558.
[13] A.J. Medford, J. Wellendorff, A. Vojvodic, F. Studt, F. Abild-Pedersen, K.W. Jacobsen, T. Bligaard, J.K. Nørskov, Science 345 (2014) 197–200.
[14] H. Öström, H. Öberg, H. Xin, J. LaRue, M. Beye, M. Dell'Angela, J. Gladh, M.L. Ng, J.A. Sellberg, S. Kaya, G. Mercurio, D. Nordlund, M. Hantschmann, F. Hieke, D. Kühn, W.F. Schlotter, G.L. Dakovski, J.J. Turner, M.P. Minitti, A. Mitra, S.P. Moeller, A. Föhlisch, M. Wolf, W. Wurth, M. Persson, J.K. Nørskov, F. Abild-Pedersen, H. Ogasawara, L.G.M. Pettersson, A. Nilsson, Science 347 (2015) 978–982.
[15] F. Studt, F. Abild-Pedersen, T. Bligaard, R.Z. Sorensen, C.H. Christensen, J.K. Norskov, Science 320 (2008) 1320–1322.
[16] A. Villa, N. Dimitratos, C.E. Chan-Thaw, C. Hammond, G.M. Veith, D. Wang, M. Manzoli, L. Prati, G.J. Hutchings, Chem. Soc. Rev. 45 (2016) 4953–4994.
[17] J. Dou, Z. Sun, A.A. Opalade, N. Wang, W. Fu, F.F. Tao, Chem. Soc. Rev. 46 (2017) 2001–2027.
[18] C.H. van Oversteeg, H.Q. Doan, F.M. de Groot, T. Cuk, Chem. Soc. Rev. 46 (2017) 102–125.
[19] W. Gao, Z.D. Hood, M. Chi, Acc. Chem. Res. 50 (2017) 787–795.
[20] P. Serna, A. Corma, ACS Catal. 5 (2015) 7114–7121.
[21] E.A. Gelder, S.D. Jackson, C.M. Lok, Chem. Commun. 4 (2005) 522–524.
[22] H.U. Blaser, H. Steiner, M. Studer, ChemCatChem 1 (2009) 210–221.
[23] Q.H. Cui, L. Jiang, C. Zhang, Y.S. Zhao, W. Hu, J. Yao, Adv. Mater. 24 (2012) 2332–2336.
[24] A. Grirrane, A. Corma, H. Garcia, Gold-catalyzed synthesis of aromatic azo compounds from anilines and nitroaromatics, Science 322 (2008) 1661–1664.
[25] G. Chen, C. Xu, X. Huang, J. Ye, L. Gu, G. Li, Z. Tang, B. Wu, H. Yang, Z. Zhao, Z. Zhou, G. Fu, N. Zheng, Nat. Mater. 15 (2016) 564–569.
[26] P. Serna, P. Concepción, A. Corma, J. Catal. 265 (2009) 19–25.
[27] M. Boronat, F. Illas, A. Corma, J. Phys. Chem. A 113 (2009) 3750–3757.
[28] D. Combita, P. Concepcion, A. Corma, J. Catal. 311 (2014) 339–349.
[29] Q. Zhang, X. Li, Q. Ma, Q. Zhang, H. Bai, W. Yi, J. Liu, J. Han, G. Xi, Nat. Commun. 8 (2017) 149031–149039.
[30] Z.-F. Huang, J. Song, X. Wang, L. Pan, K. Li, X. Zhang, L. Wang, J.-J. Zou, Nano

Energy 40 (2017) 308–316.
[31] Z.-F. Huang, J. Song, L. Pan, F. Lv, Q. Wang, J.-J. Zou, X. Zhang, L. Wang, Chem. Commun. 50 (2014) 10959–10962.
[32] J. Song, Z.-F. Huang, L. Pan, J.-J. Zou, X. Zhang, L. Wang, ACS Catal. 5 (2015) 6594–6599.
[33] J. Lu, J. Song, H. Niu, L. Pan, X. Zhang, L. Wang, J.-J. Zou, Appl. Surf. Sci. 371 (2016) 61–66.
[34] Y.-C. Zhang, L. Pan, J. Lu, J. Song, Z. Li, X. Zhang, L. Wang, J.-J. Zou, Appl. Surf. Sci. 401 (2017) 241–247.
[35] Z. Wu, Y. Cheng, F. Tao, L. Daemen, G.S. Foo, L. Nguyen, X. Zhang, A. Beste, A.J. Ramirez-Cuesta, J. Am. Chem. Soc. 139 (2017) 9721–9727.
[36] R.S. Downing, P.J. Kunkeler, H. van Bekkum, Catal. Today 37 (1997) 121–136.
[37] Y.J. Shu, H.C. Chan, L.F. Xie, Z.P. Shi, Y. Tang, Q.S. Gao, ChemCatChem 9 (2017) 4199–4205.
[38] D.M. Nevskaia, E. Castillejos-Lopez, V. Munoz, A. Guerrero-Ruiz, Environ. Sci. Technol. 38 (2004) 5786–5796.
[39] L. He, F. Weniger, H. Neumann, M. Beller, Angew. Chem. Int. Ed. 55 (2016) 12582–12594.
[40] H. Wei, X. Liu, A. Wang, L. Zhang, B. Qiao, X. Yang, Y. Huang, S. Miao, J. Liu, T. Zhang, Nat. Commun. 5 (2014) 56341–56348.
[41] Y. Ren, H. Wei, G. Yin, L. Zhang, A. Wang, T. Zhang, Chem. Commun. 53 (2017) 1969–1972.
[42] P.R. Chen, F.K. Yang, A. Kostka, W. Xia, ACS Catal. 4 (2014) 1478–1486.
[43] L. Shang, T. Bian, B. Zhang, D. Zhang, L.Z. Wu, C.H. Tung, Y. Yin, T. Zhang, Angew. Chem. Int. Ed. 53 (2014) 250–254.
[44] L. Shang, Y.H. Liang, M.Z. Li, G.I.N. Waterhouse, P. Tang, D. Ma, L.Z. Wu, C.H. Tung, T.R. Zhang, Adv. Funct. Mater. 27 (2017), http://dx.doi.org/10.1002/adfm.201606215.
[45] P. Liu, R. Qin, G. Fu, N. Zheng, J. Am. Chem. Soc. 139 (2017) 2122–2131.
[46] A.T. Bell, 299 (2003), 1688–1691.
[47] P. Zhang, C. Yu, X. Fan, X. Wang, Z. Ling, Z. Wang, J. Qiu, Phys. Chem. Chem. Phys. 17 (2015) 145–150.
[48] N. Mahata, A.F. Cunha, J.J.M. Orfao, J.L. Figueiredo, Appl. Catal. A 351 (2008) 204–209.
[49] G. Hahn, J.K. Ewert, C. Denner, D. Tilgner, R. Kempe, ChemCatChem 8 (2016) 2461–2465.
[50] T. Schwob, R. Kempe, Angew. Chem. Int. Ed. 55 (2016) 15175–15179.
[51] R. Raja, V.B. Golovko, J.M. Thomas, A. Berenguer-Murcia, W. Zhou, S. Xie, B.F. Johnson, Chem. Commun. 15 (2005) 2026–2028.
[52] B. Qiao, A. Wang, X. Yang, L.F. Allard, Z. Jiang, Y. Cui, J. Liu, J. Li, T. Zhang, Nat. Chem. 3 (2011) 634–641.
[53] X.F. Yang, A. Wang, B. Qiao, J. Li, J. Liu, T. Zhang, Acc. Chem. Res. 46 (2013) 1740–1748.
[54] W.G. Liu, L.L. Zhang, W.S. Yan, X.Y. Liu, X.F. Yang, S. Miao, W.T. Wang, A.Q. Wang, T. Zhang, Chem. Sci. 7 (2016) 5758–5764.
[55] T.Y. Cheng, H. Yu, F. Peng, H.J. Wang, B.S. Zhang, D.S. Su, Catal. Sci. Technol. 6 (2016) 1007–1015.
[56] S. Zhang, C.R. Chang, Z.Q. Huang, J. Li, Z. Wu, Y. Ma, Z. Zhang, Y. Wang, Y. Qu, J. Am. Chem. Soc. 138 (2016) 2629–2637.
[57] P. Liu, Y. Zhao, R. Qin, S. Mo, G. Chen, L. Gu, D.M. Chevrier, P. Zhang, Q. Guo, D. Zang, B. Wu, G. Fu, N. Zheng, Science 352 (2016) 797–801.
[58] B. Zhang, H. Asakura, J. Zhang, J. Zhang, S. De, N. Yan, Angew. Chem. Int. Ed. 55 (2016) 8319–8323.
[59] X. Huang, Y. Li, Y. Li, H. Zhou, X. Duan, Y. Huang, Synthesis of PtPd bimetal nanocrystals with controllable shape, composition, and their tunable catalytic properties, Nano. Lett. 12 (2012) 4265–4270.
[60] F. Cardenas-Lizana, S. Gomez-Quero, A. Hugon, L. Delannoy, C. Louis, M.A. Keane, J. Catal. 262 (2009) 235–243.
[61] Z.-F. Huang, J. Wang, Y. Peng, C.-Y. Jung, A. Fisher, X. Wang, Adv. Energy Mater. (2017) 1700544.
[62] L. Bu, N. Zhang, S. Guo, X. Zhang, J. Li, J. Yao, T. Wu, G. Lu, J.Y. Ma, D. Su, X. Huang, Science 354 (2016) 1410–1414.
[63] H. Huang, H. Jia, Z. Liu, P. Gao, J. Zhao, Z. Luo, J. Yang, J. Zeng, Angew. Chem. Int. Ed. 56 (2017) 3594–3598.
[64] J. Mao, W. Chen, W. Sun, Z. Chen, J. Pei, D. He, C. Lv, D. Wang, Y. Li, Angew. Chem. Int. Ed. 56 (2017) 1197–11975.
[65] J. Wu, L. Qi, H. You, A. Gross, J. Li, H. Yang, J. Am. Chem. Soc. 134 (2012) 11880–11883.
[66] L. Wang, S. Zhao, C. Liu, C. Li, X. Li, H. Li, Y. Wang, C. Ma, Z. Li, J. Zeng, Nano. Lett. 15 (2015) 2875–2880.
[67] L. Bu, S. Guo, X. Zhang, X. Shen, D. Su, G. Lu, X. Zhu, J. Yao, J. Guo, X. Huang, Nat. Commun. 7 (2016) 118501–1185010.
[68] C.W. Jones, K. Tsuji, M.E. Davis, Nature 393 (1998) 52–54.
[69] J. Zhang, L. Wang, Y. Shao, Y. Wang, B.C. Gates, F.-S. Xiao, Angew. Chem. Int. Ed. 129 (2017) 9879–9883.
[70] M.S. Xie, B.Y. Xia, Y.W. Li, Y. Yan, Y.H. Yang, Q. Sun, S.H. Chan, A. Fisher, X. Wang, Energy Environ. Sci. 9 (2016) 1687–1695.
[71] J.B. Ernst, C. Schwermann, G.-i. Yokota, M. Tada, S. Muratsugu, N.L. Doltsinis, F. Glorius, J. Am. Chem. Soc. 139 (2017) 9144–9147.
[72] J.C. Matsubu, S. Zhang, L. DeRita, N.S. Marinkovic, J.G. Chen, G.W. Graham, X. Pan, P. Christopher, Nat. Chem. 9 (2017) 120–127.
[73] M. Makosch, J. Sá, C. Kartusch, G. Richner, J.A. vanBokhoven, K. Hungerbühler, ChemCatChem 4 (2012) 59–63.
[74] Z.-F. Huang, J. Song, L. Pan, X. Zhang, L. Wang, J.-J. Zou, Adv. Mater. 27 (2015) 5309–5327.
[75] Z.-F. Huang, J. Song, L. Pan, X. Jia, Z. Li, J.-J. Zou, X. Zhang, L. Wang, Nanoscale 6 (2014) 8865–8872.
[76] Z.-F. Huang, J.-J. Zou, L. Pan, S. Wang, X. Zhang, L. Wang, Appl. Catal. B: Environ. 147 (2014) 167–174.
[77] H.L. Niu, J.H. Lu, J.-J. Song, L. Pan, X. Zhang, L. Wang, J.-J. Zou, Ind. Eng. Chem. Res. 55 (2016) 8527–8533.
[78] G. Vile, B. Bridier, J. Wichert, J. Perez-Ramirez, Angew. Chem. Int. Ed. 51 (2012) 8620–8623.
[79] G. Vile, S. Colussi, F. Krumeich, A. Trovarelli, J. Perez-Ramirez, Angew. Chem. Int. Ed. 53 (2014) 12069–12072.
[80] O. Martin, A.J. Martin, C. Mondelli, S. Mitchell, T.F. Segawa, R. Hauert, C. Drouilly, D. Curulla-Ferre, J. Perez-Ramirez, Angew. Chem. Int. Ed. 55 (2016) 6261–6265.
[81] D. Albani, M. Capdevila-Cortada, G. Vile, S. Mitchell, O. Martin, N. Lopez, J. Perez-Ramirez, Angew. Chem. Int. Ed. 56 (2017) 10755–10760.
[82] I.A. de Castro, R.S. Datta, J.Z. Ou, A. Castellanos-Gomez, S. Sriram, T. Daeneke, K. Kalantar-Zadeh, Adv. Mater. 29 (2017), http://dx.doi.org/10.1002/adma.201701619.
[83] S. Pisiewicz, D. Formenti, A.E. Surkus, M.M. Pohl, J. Radnik, K. Junge, C. Topf, S. Bachmann, M. Scalone, M. Beller, ChemCatChem 8 (2016) 129–134.
[84] T. Stemmler, A.E. Surkus, M.M. Pohl, K. Junge, M. Beller, ChemSusChem 7 (2014) 3012–3016.
[85] R.V. Jagadeesh, T. Stemmler, A.E. Surkus, M. Bauer, M.M. Pohl, J. Radnik, K. Junge, H. Junge, A. Bruckner, M. Beller, Nat. Protoc. 10 (2015) 916–926.
[86] R.V. Jagadeesh, T. Stemmler, A.-E. Surkus, H. Junge, K. Junge, M. Beller, Nat. Protoc. 10 (2015) 548–557.
[87] R.V. Jagadeesh, K. Murugesan, A.S. Alshammari, H. Neumann, M.M. Pohl, J. Radnik, M. Beller, Science 358 (2017) 326–332.
[88] F. Cao, R.X. Liu, L. Zhou, S.Y. Song, Y.Q. Lei, W.D. Shi, F.Y. Zhao, H.J. Zhang, J. Mater. Chem. 20 (2010) 1078–1085.
[89] V. Kratky, M. Kralik, M. Mecarova, M. Stolcova, L. Zalibera, M. Hronec, Appl. Catal. A 235 (2002) 225–231.
[90] N. Perret, A.M. Alexander, S.M. Hunter, P. Chung, J.S.J. Hargreaves, R.F. Howe, M.A. Keane, Appl. Catal. A 488 (2014) 128–137.
[91] Y. Zhu, F. Liu, W. Ding, X. Guo, Y. Chen, Angew. Chem. Int. Ed. 45 (2006) 7211–7214.
[92] M. Mo, L. Han, J. Lv, Y. Zhu, L. Peng, X. Guo, W. Ding, Chem. Commun. 46 (2010) 2268–2270.
[93] H. Li, Q. Zhao, Y. Wan, W. Dai, M. Qiao, J. Catal. 244 (2006) 251–254.
[94] Z.K. Zhao, H.L. Yang, Y. Li, RSC Adv. 4 (2014) 22669–22677.
[95] T. Fu, M. Wang, W.M. Cai, Y.M. Cui, F. Gao, L.M. Peng, W. Chen, W.P. Ding, ACS Catal. 4 (2014) 2536–2543.
[96] Y. Xu, Y. Mo, J. Tian, P. Wang, H. Yu, J. Yu, Appl. Catal. B: Environ. 181 (2016) 810–817.
[97] J. Wang, K. Wang, F.B. Wang, X.H. Xia, Nat. Commun. 5 (2014) 52851–528519.
[98] R. Gao, L. Pan, J. Lu, J. Xu, X. Zhang, L. Wang, J.-J. Zou, ChenCatChem 9 (2017) 4287–4294.
[99] T. Wang, Z. Dong, T. Fu, Y. Zhao, T. Wang, Y. Wang, Y. Chen, B. Han, W. Ding, Chem. Commun. 51 (2015) 17712–17715.
[100] Z. Wei, J. Wang, S. Mao, D. Su, H. Jin, Y. Wang, F. Xu, H. Li, Y. Wang, ACS Catal. 5 (2015) 4783–4789.
[101] D.S. Su, S. Perathoner, G. Centi, Nanocarbons for the development of advanced catalysts, Chem. Rev. 113 (2013) 5782–5816.
[102] F. Leng, I.C. Gerber, P. Lecante, S. Moldovan, M. Girleanu, M.R. Axet, P. Serp, ACS Catal. 6 (2016) 6018–6024.
[103] B. Li, Z. Xu, J. Am. Chem. Soc. 131 (2009) 16380–16382.
[104] L. Pacosová, C. Kartusch, P. Kukula, J.A. vanBokhoven, ChemCatChem 3 (2011) 154–156.
[105] G. Brieger, T.J. Nestrick, Chem. Rev. 74 (1974) 567–580.
[106] D. Wang, D. Astruc, Chem. Rev. 115 (2015) 6621–6686.
[107] M.J. Gilkey, B.J. Xu, ACS Catal. 6 (2016) 1420–1436.
[108] Y. Gao, D. Ma, C. Wang, J. Guan, X. Bao, Chem. Commun. 47 (2011) 2432–2434.
[109] Z.K. Zhao, H.L. Yang, Y. Li, X.W. Guo, Green Chem. 16 (2014) 1274–1281.
[110] D. Cantillo, M. Baghbanzadeh, C.O. Kappe, Angew. Chem. Int. Ed. 51 (2012) 10190–10193.
[111] B. Yang, Q.K. Zhang, X.Y. Ma, J.Q. Kang, J.M. Shi, B. Tang, Nano Res. 9 (2016) 1879–1890.
[112] P.S. Kumbhar, J. Sanchez-Valente, J.M.M. Millet, F. Figueras, J. Catal. 191 (2000) 467–473.
[113] R.V. Jagadeesh, G. Wienhofer, F.A. Westerhaus, A.E. Surkus, M.M. Pohl, H. Junge, K. Junge, M. Beller, Chem. Commun. 47 (2011) 10972–10974.
[114] H.Z. Zhu, Y.M. Lu, F.J. Fan, S.H. Yu, Nanoscale 5 (2013) 7219–7223.
[115] H. Yang, X. Cui, X. Dai, Y. Deng, F. Shi, Nat. Commun. 6 (2015) 6478.
[116] S. Wu, G. Wen, J. Wang, J. Rong, B. Zong, R. Schlögl, D.S. Su, Catal. Sci. Technol. 4 (2014) 4183–4187.
[117] D.S. Su, S. Perathoner, G. Centi, Chem. Rev. 113 (2013) 5782–5816.
[118] S. Fujita, H. Watanabe, A. Katagiri, H. Yoshida, M. Arai, J. Mol. Catal. A 393 (2014) 257–262.
[119] C. Zhang, J. Lu, M. Li, Y. Wang, Z. Zhang, H. Chen, F. Wang, Green Chem. 18 (2016) 2435–2442.
[120] L. He, Y. Huang, A. Wang, X. Wang, X. Chen, J.J. Delgado, T. Zhang, Angew. Chem. Int. Ed. 51 (2012) 6191–6194.
[121] O. Marin-Flores, T. Turba, C. Ellefson, K. Wang, J. Breit, J. Ahn, M.G. Norton, S. Ha, Appl. Catal. B-Environ. 98 (2010) 186–192.
[122] A.K. Patra, A. Dutta, A. Bhaumik, Catal. Commun. 11 (2010) 651–655.
[123] W.W. Lin, H.Y. Cheng, J. Ming, Y.C. Yu, F.Y. Zhao, J. Catal. 291 (2012) 149–154.
[124] Y.K. Park, S.B. Choi, H.J. Nam, D.Y. Jung, H.C. Ahn, K. Choi, H. Furukawa, J. Kim,

Chem. Commun. 46 (2010) 3086–3088.
[125] A.W. Peters, Z. Li, O.K. Farha, J.T. Hupp, ACS Nano 9 (2015) 8484–8490.
[126] X.-F. Yu, L.-B. Mao, J. Ge, Z.-L. Yu, J.-W. Liu, S.-H. Yu, Sci. Bull. 61 (2016) 700–705.
[127] F. Wang, S. Song, K. Li, J. Li, J. Pan, S. Yao, X. Ge, J. Feng, X. Wang, H. Zhang, Adv. Mater. 28 (2016) 10679–10683.
[128] Y. Su, J. Lang, L. Li, K. Guan, C. Du, L. Peng, D. Han, X. Wang, J. Am. Chem. Soc. 135 (2013) 11433–11436.
[129] M. Shalom, V. Molinari, D. Esposito, G. Clavel, D. Ressnig, C. Giordano, M. Antonietti, Adv. Mater. 26 (2014) 1272–1276.
[130] Z. Li, Q. Xu, Acc. Chem. Res. 50 (2017) 1449–1458.
[131] R.V. Jagadeesh, K. Natte, H. Junge, M. Beller, ACS Catal. 5 (2015) 1526–1529.
[132] R.V. Jagadeesh, D. Banerjee, P.B. Arockiam, H. Junge, K. Junge, M.M. Pohl, J. Radnik, A. Bruckner, M. Beller, Green Chem. 17 (2015) 898–902.
[133] I. Sorribes, G. Wienhofer, C. Vicent, K. Junge, R. Llusar, M. Beller, Angew. Chem. Int. Ed. 51 (2012) 7794–7798.
[134] M.S. Li, Y.F. Hao, F. Cardenas-Lizana, H.H.P. Yiu, M.A. Keane, Top. Catal. 58 (2015) 149–158.
[135] J. Long, Y. Zhou, Y. Li, Transfer hydrogenation of unsaturated bonds in the absence of base additives catalyzed by a cobalt-based heterogeneous catalyst, Chem. Commun. 51 (2015) 2331–2334.
[136] J.E. Trancik, Nature 507 (2014) 300–302.
[137] N. Zhang, M.Q. Yang, S. Liu, Y. Sun, Y.J. Xu, Chem. Rev. 115 (2015) 10307–10377.
[138] K. Imamura, K. Hashimoto, H. Kominami, Chem. Commun. 48 (2012) 4356–4358.
[139] Y. Shiraishi, H. Hirakawa, Y. Togawa, Y. Sugano, S. Ichikawa, T. Hirai, ACS Catal. 3 (2013) 2318–2326.
[140] Y. Shiraishi, Y. Togawa, D. Tsukamoto, S. Tanaka, T. Hirai, ACS Catal. 2 (2012) 2475–2481.
[141] F. Mahdavi, T.C. Bruton, Y. Li, J. Org. Chem. 58 (1993) 744–746.
[142] H.Q. Wang, J.P. Yan, W.F. Chang, Z.M. Zhang, Catal. Commun. 10 (2009) 989–994.
[143] S. Fuldner, R. Mild, H.I. Siegmund, J.A. Schroeder, M. Gruber, B. Konig, Green Chem. 12 (2010) 400–406.
[144] J.L. Ferry, W.H. Glaze, Langmuir 14 (1998) 3551–3555.
[145] X. Chen, S. Mao, Chem. Rev. 107 (2007) 2891–2959.
[146] X. Chen, L. Liu, P.Y. Yu, S.S. Mao, Science 331 (2011) 746–750.
[147] T.L. Thompson, J.T. Yates Jr., Chem. Rev. 106 (2006) 4428–4453.
[148] U. Diebold, Surf. Sci. Rep. 48 (2003) 53–229.
[149] N. Zhang, Y.H. Zhang, X.Y. Pan, X. Fu, S. Liu, Y.-J. Xu, J. Phys. Chem. C 115 (2011) 23501–23511.
[150] F.X. Xiao, J. Miao, B. Liu, J. Am. Chem. Soc. 136 (2014) 1559–1569.
[151] L. Liu, X. Zhang, L. Yang, L. Ren, D. Wang, J. Ye, Natl. Sci. Rev. 0 (2017) 1–20.
[152] H. Tada, T. Ishida, A. Takao, S. Ito, Langmuir 20 (2004) 7898–7900.
[153] S. Naya, T. Niwa, T. Kume, H. Tada, Angew. Chem. Int. Ed. 53 (2014) 7305–7309.
[154] H. Zhu, X. Ke, X. Yang, S. Sarina, H. Liu, Angew. Chem. Int. Ed. 49 (2010) 9657–9661.
[155] C. Wang, D. Astruc, Chem. Soc. Rev. 43 (2014) 7188–7216.
[156] X.M. Zhou, G. Liu, J.G. Yu, W.H. Fan, J. Mater. Chem. 22 (2012) 21337–21354.
[157] Y. Zhang, X. Cui, F. Shi, Y. Deng, Chem. Rev. 112 (2012) 2467–2505.
[158] X. Guo, C. Hao, G. Jin, H.Y. Zhu, X.Y. Guo, Angew. Chem. Int. Ed. 53 (2014) 1973–1977.
[159] S.W. Hsu, K. On, A.R. Tao, J. Am. Chem. Soc. 133 (2011) 19072–19075.
[160] A. Furube, L. Du, K. Hara, R. Katoh, M. Tachiya, J. Am. Chem. Soc. 129 (2007) 14852–14853.
[161] J. Cui, Y. Li, L. Liu, L. Chen, J. Xu, J. Ma, G. Fang, E. Zhu, H. Wu, L. Zhao, L. Wang, Y. Huang, Nano Lett. 15 (2015) 6295–6301.
[162] X. Lang, X. Chen, J. Zhao, Chem. Soc. Rev. 43 (2014) 473–486.
[163] C. Zhang, Y. Zhu, Chem. Mater. 17 (2005) 3537–3545.
[164] T. Kamegawa, H. Seto, S. Matsuura, H. Yamashita, ACS Appl. Mater. Interfaces 4 (2012) 6635–6639.
[165] S. Füldner, R. Mild, H.I. Siegmund, J.A. Schroeder, M. Gruber, B. König, Green Chem. 12 (2010) 400–406.
[166] S. Füldner, T. Mitkina, T. Trottmann, A. Frimberger, M. Gruber, B. König, Photochem. Photobiol. Sci. 10 (2011) 623–625.
[167] D.A. Nicewicz, D.W. MacMillan, Science 322 (2008) 77–80.
[168] T.P. Yoon, M.A. Ischay, J.N. Du, Nat. Chem. 2 (2010) 527–532.
[169] H.W. Shih, M.N. Vander Wal, R.L. Grange, D.W. MacMillan, J. Am. Chem. Soc. 132 (2010) 13600–13603.
[170] M. Neumann, S. Fuldner, B. Konig, K. Zeitler, Angew. Chem. Int. Ed. 50 (2011) 951–954.
[171] X.J. Yang, B. Chen, L.Q. Zheng, L.Z. Wu, C.H. Tung, Green Chem. 16 (2014) 1082–1086.
[172] D.D. Zhu, J.L. Liu, S.Z. Qiao, Adv. Mater. 28 (2016) 3423–3452.
[173] C. Liu, A.Y. Zhang, D.N. Pei, H.Q. Yu, Environ. Sci. Technol. 50 (2016) 5234–5242.
[174] B. Wouters, X. Sheng, A. Boschin, T. Breugelmans, E. Ahlberg, I.F.J. Vankelecom, P.P. Pescarmona, A. Hubin, Electrochim. Acta 111 (2013) 405–410.
[175] Y. Wang, Y.G. Chen, C.Y. Nan, L.L. Li, D.S. Wang, Q. Peng, Y.D. Li, Nano Res. 8 (2015) 140–155.
[176] J. Jiang, R. Zhai, X. Bao, J. Alloys Compounds 354 (2003) 248–258.
[177] F.D. Popp, H.P. Schultz, Chem. Rev. 62 (1962) 19–40.
[178] G. Seshadri, J.A. Kelber, J. Electrochem. Soc. 146 (1999) 3762–3764.
[179] J. Marquez, D. Pletcher, J. Appl. Electrochem. 10 (1980) 567–573.
[180] K. Polat, M.L. Aksu, A.T. Pekel, J. Appl. Electrochem. 32 (2002) 217–223.
[181] A. Cyr, P. Huot, J.F. Marcoux, G. Belot, E. Laviron, J. Lessard, Electrochim. Acta 34 (1989) 439–445.
[182] A. Cyr, P. Huot, G. Belot, J. Lessard, Electrochim. Acta 35 (1990) 147–152.
[183] L.Z. Huang, H.C. Hansen, M.J. Bjerrum, J. Hazard. Mater. 306 (2016) 175–183.
[184] Y. Zhang, X. Bo, A. Nsabimana, C. Han, M. Li, L. Guo, J. Mater. Chem. A 3 (2015) 732–738.
[185] Y. Sang, B. Wang, Q. Wang, G. Zhao, P. Guo, Sci. Rep. 4 (2014) 63211–63216.
[186] D. Zhang, C. Zhou, Z. Sun, L.Z. Wu, C.H. Tung, T. Zhang, Nanoscale 4 (2012) 6244–6255.

Dr. Jiajia Song received her Ph.D degree in School of Chemical Engineering and Technology, Tianjin University, China, under the supervision of Prof. Ji-Jun Zou, in 2017, respectively. She is currently a postdoctoral research fellow in Cambridge Centre of Advanced Research in Energy Efficiency in Singapore (CARES), Singapore. Her research interests mainly focus on combining theoretic computation and experimental methods to study the activity origin and design the new hydrogenation catalysts at the level surface and interface.

Dr. Zhen-Feng Huang received his Ph.D and M.S. degrees in School of Chemical Engineering and Technology, Tianjin University, China, in 2016, under the supervision of Prof. Ji-Jun Zou. He is currently a postdoctoral research fellow in School of Chemical and Biomedical Engineering, Nanyang Technological University, Singapore. His research interests mainly focus on the design and synthesis of nanomaterials for catalytic hydrogenation, photocatalysis and electrocatalysis.

Dr. Lun Pan received his B.S. and Ph.D. degrees in School of Chemical Engineering and Technology, Tianjin University, China, in 2009 and 2014, respectively, under the supervision of Prof. Xiangwen Zhang and Prof. Ji-Jun Zou. Then he became an assistant professor at School of Chemical Engineering and Technology, Tianjin University. His research interests include the design and synthesis of nanostructured materials for photocatalysis, electrocatalysis and piezo-phototronics.

Miss Ke Li received her B.S. degree in School of Chemical Engineering and Technology, Tianjin University, China, in 2016, and then became a M.S. candidate under the supervision of Prof. Ji-Jun Zou at School of Chemical Engineering and Technology, Tianjin University, China. Her research interests mainly focus on the design and synthesis of nanomaterials for photocatalytic and electrocatalytic water splitting and electrocatalytic oxygen reduction.

Prof. Xiangwen Zhang received his B.S. and M.S. degree in chemical engineering from Tianjin University in 1984 and 1987, respectively, under the supervision of Prof. Hongfang Chen, and then became a research assistant at School of Chemical Engineering. He received Ph.D. in 2003 and become a full professor from 2006. His research interests include fuel processing technology and reaction engineering.

Prof. Li Wang received her Ph.D. degree in chemical engineering from Tianjin University in 1999. After working as post-doctor for 2 years at School of Chemical Engineering, she became an associated professor of Tianjin University and was promoted as full professor in 2008. She was the visiting scholar from 2006 to 2007 at Institute of Chemical engineering, RWTH Aachen University. Her research interests include petrochemical technology, reaction engineering and separation processes.

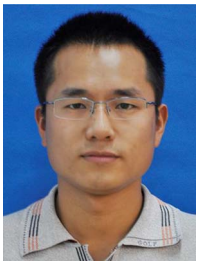

Prof. Ji-Jun Zou received his B.S., M.S. and Ph.D. degrees in chemical engineering from Tianjin University in 2000, 2002 and 2005, respectively. Then he became an assistant professor at School of Chemical Engineering and Technology, Tianjin University and was promoted as full professor from 2013. His research interests mainly surround nanostructured catalysts for photo/electrocatalysis, fuel processing and biomass conversion. He received several awards including National Excellent Young Scientist (by NSFC), Changjiang Young Scholar (by MOE), National Excellent Doctoral Dissertation (by MOE) and Peiyang Distinguished Young Scholar (by TJU).